Satellite Galaxies and Fossil Groups in the Millennium Simulation

Laura V. Sales[1,2], Julio F. Navarro[3,4]⋆, Diego G. Lambas[1,2], Simon D. M. White[4] &
Darren J. Croton[5]

[1] *Observatorio Astronómico, Universidad Nacional de Córdoba, Laprida 854, 5000 Córdoba, Argentina.*
[2] *Instituto de Astronomía Teórica y Experimental, Conicet, Argentina.*
[3] *Department of Physics and Astronomy, University of Victoria, B.C., Canada.*
[4] *Max-Planck-Institut für Astrophysik, D-85740 Garching, Germany.*
[5] *Department of Astronomy, University of California, Berkeley, CA, 94720, USA.*

28 October 2018

ABSTRACT

We use a semianalytic galaxy catalogue constructed from the *Millennium Simulation* (*MS*) to study the satellites of isolated galaxies in the ΛCDM cosmogony. The large volume surveyed by the *MS* ($500^3 \, h^{-3} \mathrm{Mpc}^3$), together with its unprecedented numerical resolution, enable the compilation of a large sample of $\sim 80,000$ bright ($M_r < -20.5$) primaries, surrounded by $\sim 178,000$ satellites down to the faint magnitude limit ($M_r = -17$) of our catalogue. This sample allows the characterization, with minimal statistical uncertainty, of the dynamical properties of satellite/primary galaxy systems in a ΛCDM universe. The details of this characterization are sensitive to the details of the modeling, such as its assumptions on galaxy merging and dynamical friction timescales, but many of its general predictions should be applicable to hierarchical formation models such as ΛCDM. We find that, overall, the satellite population traces the dark matter rather well: its spatial distribution and kinematics may be approximated by an NFW profile with a mildly anisotropic velocity distribution. Their spatial distribution is also mildly anisotropic, with a well-defined "anti-Holmberg" effect that reflects the misalignment between the major axis and angular momentum of the host halo. Our analysis also highlights a number of difficulties afflicting studies that rely on satellite velocities to constrain the primary halo mass. These arise from variations in the star formation efficiency and assembly history of isolated galaxies, which result in a scatter of up to ~ 2 decades in halo mass at fixed primary luminosity. Our isolation criterion (primaries may only have companions at least 2 mag fainter within $1 \, h^{-1}$ Mpc) contributes somewhat to the scatter, since it picks not only galaxies in sparse environments, but also a number of primaries at the centre of "fossil" groups. We find that the abundance and luminosity function of these unusual systems are in reasonable agreement with the few available observational constraints. Much tighter halo mass-luminosity relations are found when splitting the sample by colour: red primaries inhabit halos more than twice as massive as those surrounding blue primaries, a difference that vanishes, however, when considering stellar mass instead of luminosity. The large scatter in the halo mass-luminosity relation hinders the interpretation of the velocity dispersion of satellites stacked according to the luminosity of the primary. We find $L \propto \sigma^3$ (the natural scaling expected for ΛCDM) for truly-isolated primaries, i.e., systems where the central galaxy contributes more than 85% of the total luminosity within its virial radius. Less strict primary selection, however, leads to substantial modification of the scaling relation: blindly stacking satellites of all primaries results in a much shallower L-σ relation that is only poorly approximated by a power law.

Key words: galaxies: haloes - galaxies: kinematics and dynamics - dark matter - methods: statistical

1 INTRODUCTION

Satellite galaxies may be thought of as the visible fossil relics of hierarchical galaxy formation, where the mass of a galaxy is envi-

⋆ Fellow of the Canadian Institute for Advanced Research

sioned to be assembled in a sequence of accretion events. As surviving witnesses of the accretion process, satellites bear an invaluable record of the assembly history of the primary galaxy they orbit, and provide at the same time prime information about the mass and extent of the dark matter halo they inhabit.

Satellites are a particularly valuable tool for studying the outer regions of dark matter halos, where few other tracers exist that can provide effective constraints. This is especially true in the case of the Local Group, where the dynamics of the outer satellites has played an important role in mass estimates of the Milky Way and M31 (Little & Tremaine 1987; Zaritsky et al. 1989; Kochanek 1996; Wilkinson & Evans 1999; Evans & Wilkinson 2000; Battaglia et al. 2005). Local Group satellites can be found even if they are extremely faint; Draco, for example, is $\sim 8 \times 10^4$ times fainter than its primary, the Milky Way, and some of the new satellites discovered over the past few years have luminosities rivaling that of ordinary star clusters (Zucker et al. 2004, 2006; Willman et al. 2005; Martin et al. 2006; Belokurov et al. 2006, 2007; Irwin et al. 2007; Majewski et al. 2007; Ibata et al. 2007; Chapman et al. 2007).

On the other hand, extragalactic satellite studies have been traditionally limited by the scarcity of satellite/primary systems easily accessible to observation. Partly as a result of the strict isolation criteria that are imposed on the primaries in order to minimize interlopers and to avoid complications that may arise from having more than one dominant object, it is rare for primaries to have more than a few satellites bright enough for spectroscopic confirmation and follow up.

The scarcity of satellites surrounding one given primary has prompted the adoption of stacking techniques in order to overcome small number statistics. For example, the satellites of all primaries of given luminosity, L, might be combined to yield estimates of the *average*, rather than individual, halo properties as a function of L. These techniques are clearly vulnerable to the presence of luminosity-dependent biases in the satellite distribution and of systematic trends between halo mass and primary luminosity that may be difficult to detect and evaluate in observational datasets.

Such techniques, nevertheless, seem appropriate to address a number of important issues in galaxy formation studies. How does the average dark halo mass depend on the luminosity of the primary? What is the mass profile of the dark halo and how does it vary with luminosity? What is the three-dimensional shape of the dark halo and how does it relate to the primary and to the spatial distribution of satellites? These are some of the questions traditionally addressed by extragalactic satellite studies, and there is a rich literature documenting prior attempts at exploiting the dynamics of satellites to constrain the mass and extent of dark matter halos.

The pioneering work of Zaritsky et al. (1993, 1997a), for example, confirmed the presence of massive halos around isolated spirals, but also hinted at a few odd results that are difficult to reconcile with current galaxy formation models. For example, these authors noted that satellite velocities seemed to be independent of the luminosity of the primary, contrary to what might be naively expected from the Tully-Fisher relation. They also remarked that satellites seemed to be distributed anisotropically around the primary, in agreement with the early suggestion of Holmberg (1969).

These issues have been revisited using the much larger datasets compiled by the 2dfGRS (Colless et al. 2001) and the SDSS (York et al. 2000; Strauss et al. 2002) surveys, and broad consensus seems to be gradually emerging. In particular, McKay et al. (2002) and Prada et al. (2003) find that a well-defined trend between satellite velocities and primary luminosity *does* ap-

pear when considering samples substantially larger than the ones considered by Zaritsky et al. Better statistics have also clarified the anisotropic distribution of satellites around spirals, which, contrary to Holmberg's suggestion, apparently tend to avoid the rotation axis of the disk (Brainerd 2005; Azzaro et al. 2006; Yang et al. 2006; Agustsson & Brainerd 2007). Finally, the availability of larger samples have also enabled studies of the satellite velocity dispersion profile, which may be used to probe the outer dark mass distribution and to compare it with cosmological N-body simulations (see Prada et al. 2003, also the review of Brainerd 2004a, and van den Bosch et al. 2005a,b).

The success of these studies depends crucially on identifying and understanding possibly subtle biases between dark matter and the satellite population. This is best accomplished through direct numerical simulations, where full 3D dynamical information is available and from which mock observational datasets may be created to assess the ability of analysis techniques to identify and correct for such biases. Progress, however, has been slow, mainly because simulations with enough dynamic range to resolve simultaneously a galaxy and its satellites have only recently become possible (Klypin et al. 1999; Moore et al. 1999; Kravtsov et al. 2004; Gao et al. 2004; Diemand et al. 2004; Macciò et al. 2006; Diemand et al. 2007; Libeskind et al. 2007; Sales et al. 2007b,a). Further, these simulations have typically followed small volumes (single halos, in many cases) and many of them have focussed on the dark matter component only, hindering direct comparisons between theory and observation.

We investigate these issues here using the galaxy catalogue created by Croton et al. (2006) from the *Millennium Simulation* (Springel et al. 2005, hereafter *MS* for short). The catalogue is the result of a sophisticated semianalytic galaxy formation model applied to an N-body simulation of unprecedented dynamic range. This model has been calibrated to reproduce many of the large-scale properties of the observed galaxy population, such as the luminosity and correlation functions, as well as their color dependence. However, no specific information about satellite systems has been taken into account and, therefore, the results we present here may be considered true theoretical "predictions" that can be contrasted fruitfully with observation.

Our principal aim is to provide a detailed characterization of the 3D properties of the satellite population of bright, isolated galaxies in the ΛCDM cosmogony. This characterization is intended (i) to guide the interpretation of observational datasets, (ii) to improve the identification of primary/satellite systems so as to minimize the contamination by interlopers, and (iii) to provide a framework within which the questions posed above may be profitably addressed. The sheer size of the catalogue, which lists $\sim 10^7$ galaxies brighter than $M_r = -17$ in the $500^3 h^{-3}$ Mpc^3 volume of the *MS* [1], ensures that our results have negligible statistical uncertainty.

Our plan for the paper is as follows. After a brief description of the *MS* (§ 2.1) and of the semianalytic galaxy formation model (§ 2.2), we discuss our selection criteria for primaries and for satellites in § 2.3. Our main results are presented and discussed in § 3. We begin in § 3.1 with a discussion of the relation between halo mass, primary luminosity and color. Noting that our isolation criteria for primaries allows for the inclusion of "fossil groups" in our

---

[1] We express the present-day value of the Hubble constant as $H_0 = 100\,h$ km/s/Mpc. Throughout this paper, masses and luminosities will assume $h = 0.73$ unless otherwise specified.

sample, we compare their abundance and luminosity function to observations in § 3.2. The satellites' spatial distribution is discussed next (§ 3.3), together with their kinematics (§ 3.4). We end the discussion of our results by analyzing the relation between primary luminosity and satellite velocity dispersion (§ 3.6), as well as the presence of anisotropies (§ 3.7) in the satellite spatial distribution. We conclude with a brief summary in § 4.

2   THE CATALOGUE

2.1   The Millennium Simulation

The *Millennium Simulation* (*MS*), one of the projects of the Virgo Consortium [2], is a cosmological N-body simulation of the ΛCDM universe that follows the evolution of more than 10 billion particles in a box of 500 h^{-1} Mpc (comoving) on a side. The particle mass is $8.6 \times 10^9 \, h^{-1} M_\odot$, and particle-particle gravitational interactions are softened on scales smaller than 5 h^{-1} kpc. The simulation adopts parameters consistent with the WMAP1 results (Spergel et al. 2003; Seljak et al. 2005): $\Omega_{\rm m} = 0.25$, $\Omega_\Lambda = 0.75$, $h = 0.73$, $n = 1$, and $\sigma_8 = 0.9$ (for details see Springel et al. 2005). Data from the simulation output at 64 times spaced logarithmically in expansion factor before $z = 1$, and at approximately 200 Myr intervals thereafter. These data are used to build merger trees which encode the assembly history of each halo and its resolved substructure. These form the basis for the galaxy formation modeling. Complete data for these halo merging trees as well as for several galaxy formation models can be found at http://www.mpa-garching.mpg.de/millennium. The $z = 0$ data from the Croton et al (2006) model used here can be found at http://www.mpa-garching.mpg.de/galform/agnpaper/.

2.2   The Semianalytic Model

The information contained in the *MS* is harvested using semianalytic galaxy formation models that follow, with simple, but physically motivated, laws the formation of galaxies within the evolving dark matter halos. The actual prescriptions used derive from the work of Kauffmann et al. (1999), Springel et al. (2001) and De Lucia et al. (2004), but have been reformulated in the model of Croton et al (2006) to take into account newer observational constraints.

In brief, the model tracks the build-up of the luminous component of each dark matter halo by prescribing how gas cools and transforms into stars, as well as how enriched gas is devolved to the interstellar medium in halos of various masses and at different stages of the hierarchy. A novel feature of the implementation of Croton et al (2006) is the inclusion of AGN feedback to curtail star formation in massive objects and to prevent the formation of overluminous galaxies at the center of galaxy clusters. The star formation and enrichment history of galaxies is then processed with standard spectrophotometric models to provide estimates of galaxy luminosities and colors. The main data we use here is the luminosity in the 5 Sloan bands, *ugriz*, and we concentrate our analysis in the g and r bands. Unless otherwise specified, luminosities and magnitudes will refer to the r band in what follows.

The semianalytic approach follows explicitly the evolution of galaxies within dark matter halos, even when they are accreted into

(and become satellites of) larger structures. After accretion, satellite galaxies are followed consistently until their parent subhalo is destroyed by the tidal field of the more massive system, at which point the satellite orbit is subsequently identified as that of the most bound particle of the parent subhalo before disruption. The satellite is subsequently assumed to survive for some residual time consistent with dynamical friction estimates. As we shall see below, this careful treatment of the N-body simulation is crucial to characterize the dynamics of satellites of isolated galaxies in the *MS*. Some aspects of the true evolution are nevertheless neglected; in particular, the effects of dynamical friction on the orbit of a satellite after its dark halo is disrupted but before it merges with the central galaxy of its host halo, as well as a necessarily rough estimation of its merging time. This neglect will affect some aspects of the results presented below, notably the overall abundance and the radial distribution of satellites.

2.3   The Primary/Satellite Galaxy Catalogue

2.3.1   Primary galaxies

We follow standard practice and identify a sample of primary galaxies from the *MS* galaxy catalogue through (i) an *isolation* criterion, imposed to ensure that a single object dominates the local dynamics traced by the satellites, and (ii) a brightness cutoff, imposed to ensure that most primaries have a fair chance of having detectable satellites. Hereafter, we shall refer to systems brighter than $M_r = -20.5$ and surrounded, within 1 h^{-1} Mpc, *only* by companions at least 2 magnitudes fainter, as *primary galaxies*. (Note that neither the Milky Way nor M31 satisfy this strict isolation criterion.)

2.3.2   Satellites

We identify as satellites any galaxy brighter than $M_r = -17$ (the limiting magnitude of the catalogue) that lies within the virial radius [3] of a primary. Primaries with *no* satellites brighter than $M_r = -17$ within their virial radius will be referred to as *singles*. Primaries with at least one satellite will be referred to as *hosts*.

2.3.3   Further nomenclature

One complication arises from the fact that, despite our isolation criterion, some primaries might themselves be satellites of larger systems. This tends to happen in the rarefied outskirts of massive clusters. In this case, the virial radius would refer to the cluster, rather than to the parent halo of the primary, and the velocities of nearby satellites would be contaminated by high-speed cluster members. To take this into account, we shall distinguish, if pertinent, two classes of primaries: *central* and *non-central*. However, we emphasize that the fraction of non-central primaries is rather small, and that excluding them from the statistical analysis has no major influence on our main conclusions.

A second note refers to satellites, some of which, as described

---

[2] http://www.virgo.dur.ac.uk

[3] We define the *virial* radius, r_{200}, of a system as the radius of a sphere of mean density 200 times the critical density for closure, $\rho_{\rm crit} = 3H_0^2/8\pi G \sim 277.5 \, h^2 \, M_\odot/\,{\rm kpc}^3$. This implicitly defines the virial mass of a halo, M_{200}, as that enclosed within r_{200}, and the virial velocity, V_{200}, as the circular velocity measured at r_{200}. Quantities characterizing a system will be referred to as "virial" and measured within r_{200}, unless otherwise specified.
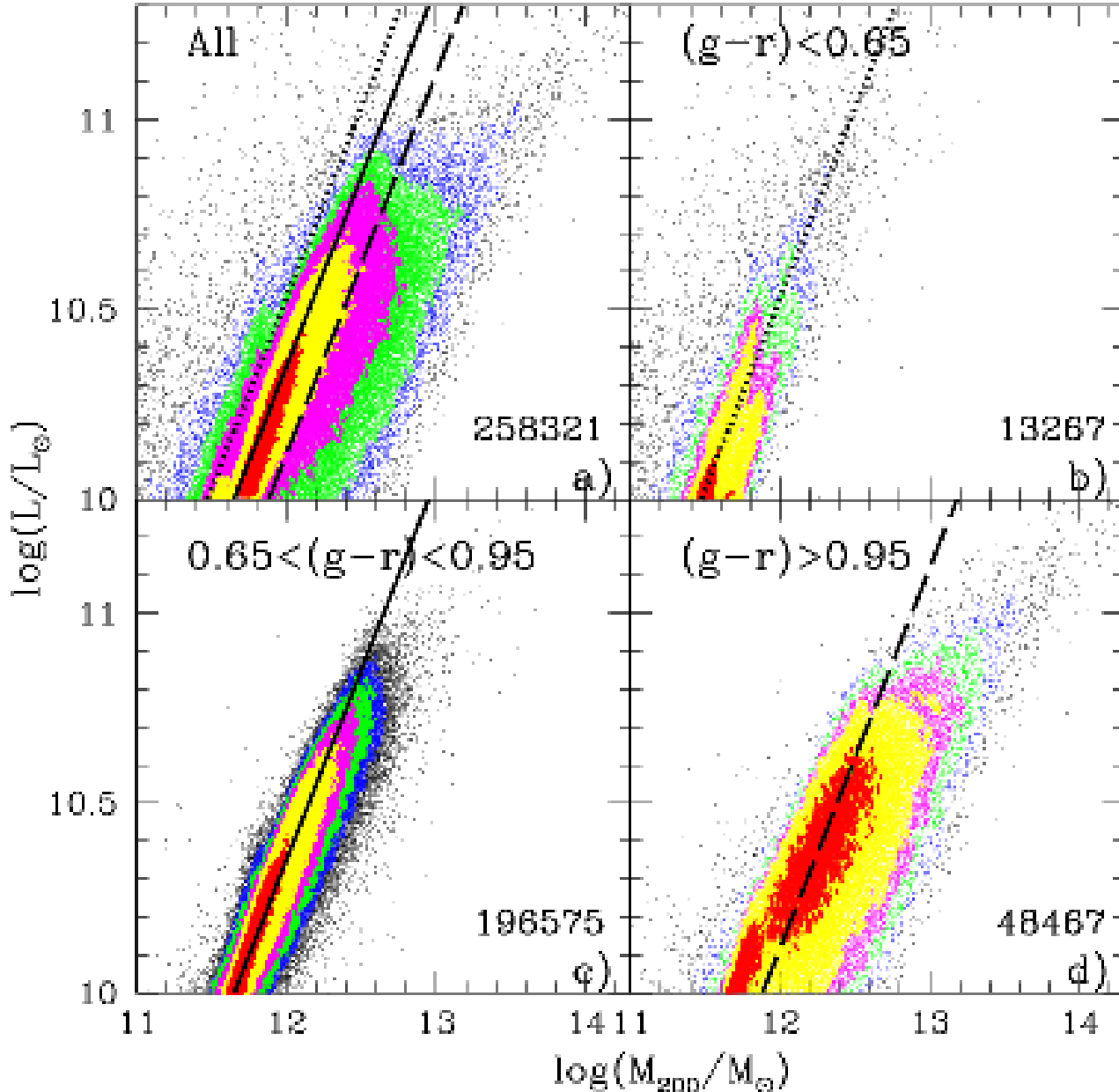
Figure 1. Virial mass vs r-band luminosity relation for primary galaxies. Panel (a) shows data for all primaries, other panels are subsamples after applying a color cut (see labels). The total number of primaries plotted in each panel is quoted. Colors indicate the density of primaries at various locations in each panel, in logarithmic units; each color step corresponds to a variation of about 10 in number. The same applies to other panels, although the color coding has been renormalized in each case to make use of the whole color palette. Dotted, solid and dashed lines indicate loci of constant virial mass-to-light ratio, and are chosen to ease the comparison between panels and to outline the presence of three "sequences" in the data (see text for further discussion).

in § 2.2, are still surrounded at the present time by their parent halos (hereafter *WSUB* satellites, for short), while others are identified with the most bound dark matter particle of the parent subhalo immediately prior to disruption (*NOSUB* satellites). Clearly, results concerning *NOSUB* satellites are likely to be more model-dependent, since the identification of the satellite as a distinct object depends in this case heavily on the assumptions made in the

model about dynamical friction timescales. It is important to keep this distinction in mind as we try and interpret the results.

2.3.4 Statistics

It is interesting to assess how our primary selection criteria select galaxies from the general population. We find that the fraction of galaxies that are designated as primaries depends only weakly on
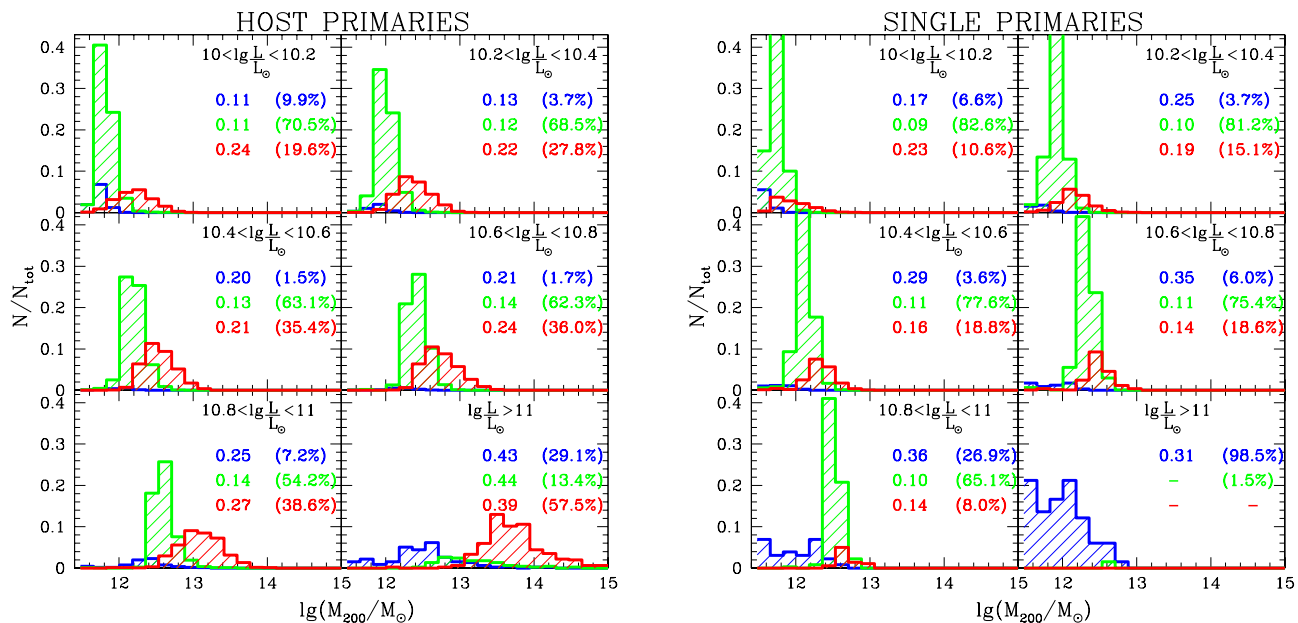
Figure 2. Virial mass distribution in luminosity bins for *host* (left panel) and *single* (right panel) primaries, split according to color (see Figure 1). Histograms have been normalized to the total number of galaxies in each luminosity bin. For *hosts* we have: $(12, 747)$, $(23, 585)$, $(26, 039)$, $(13, 817)$, $(2, 436)$ and (454) galaxies in each of the 6 bins of increasing L, respectively. For *single* primaries, the corresponding numbers are : $(91, 060)$, $(58, 364)$, $(23, 893)$, $(4, 742)$, (361) and (66), respectively. Percentages quoted in the right column of each panel indicate the fraction of primaries in each color sequence for a given luminosity bin. Left columns show the rms values $\sigma(\log(M_{200}/M_\odot))$ corresponding to each subsample.

luminosity: for example, 23% of galaxies brighter than $M_r = -23$ are *primaries*, the vast majority of which (90%) are *hosts*; 94.6% of them are of the *central* type. Fainter galaxies $(-21 < M_r < -20.5)$ have a 19% chance of being classified as *primaries*, but the majority of them (85%) are actually *singles* and therefore will not contribute to satellite studies. Of these fainter primaries, 99.5% are classified as *central*. Overall, only 1% of primaries are *non-central*, and therefore our results are unlikely to be affected by the presence of these unusual systems.

The final sample contains $258, 321$ *primaries*, $79, 000$ of which are *hosts* to at least one satellite. We find more than $178, 000$ satellites orbiting within the virial radius of the primaries, a number that rises to $508, 000$ if all satellites within $1\ h^{-1}$ Mpc of the primaries are considered. We list the fraction of primaries as a function of r-band luminosity and halo mass, along with other useful data, in Tables 1 and 2.

3 RESULTS AND DISCUSSION

3.1 Mass-Luminosity-Color relation for primaries

We begin by exploring the virial mass-luminosity relation for primaries in our catalogue, one of the main topics addressed by studies of satellite dynamics. This is shown in the top left panel of Figure 1, and illustrates the expected trend for brighter primaries to inhabit more massive halos. The most striking aspect of this figure, however, is the large scatter: at given luminosity, halos span over a decade in mass. Conversely, halos of given mass may host primaries spanning a factor of ~ 5 in luminosity. The rms deviation

at given L is substantially smaller (see table 2) but the broad tails in the mass-luminosity distribution are important, and we shall see below. The large scatter in the mass-luminosity relation reflects the variety of mass assembly and star formation histories of isolated galaxies, and must be borne in mind when "stacking" galaxies according to luminosity in order to study their average halo properties.

Different colors in Figure 1 code the number density of primaries at each location in the M-L plane, varying by a factor of ~ 10 for each step in color, and decreasing from red to blue. Most of the galaxies are in a relatively tight "main sequence" (outlined by the red dots in Figure 1 and delineated roughly by the solid line), but are surrounded by a broad cloud covering a large fraction of the panel. Closer inspection reveals the presence of two further relatively well-defined "sequences": one consisting of galaxies that are systematically brighter than the "main sequence", indicated roughly by the dotted line, and another one consisting of "underluminous" galaxies inhabiting fairly massive halos (see dashed line in Figure 1).

We note that the "main sequence" follows roughly a constant virial mass-to-light ratio. This would be the natural expectation for halos where a similar fraction of their baryonic content has been transformed into stars of roughly similar mass-to-light ratio.

The "bright sequence" (dotted line) is caused by the transient brightening of the luminous component resulting from a starburst triggered by a major merger.

The "underluminous sequence" (dashed line), on the other hand, is linked to the stunted growth of the stellar component of central galaxies in massive halos that results from the "radio-mode" AGN feedback (see for details Croton et al 2006). In such systems, halos can increase their mass substantially while their central galaxies grow only through mergers. This is indeed the way in which the
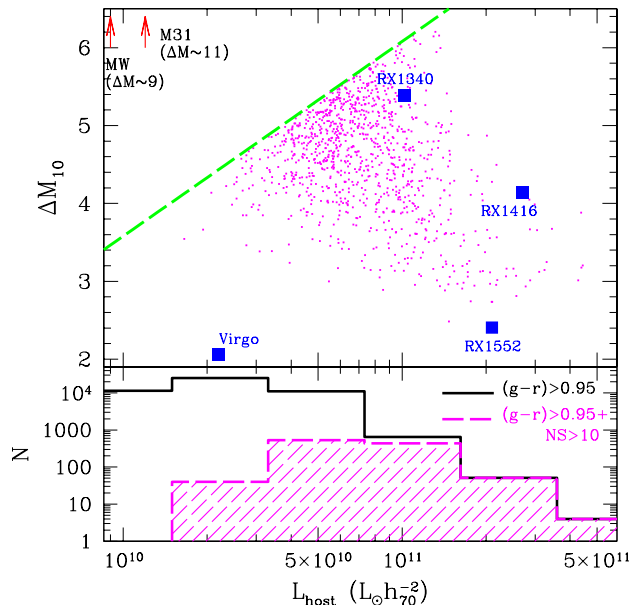
Figure 3. *Top panel:* Magnitude gap between the primary and the 10th brightest satellite within r_{200} as a function of L_{host} (expressed in units of $h_{70}^{-2} L_\odot$). The dashed line indicates the $M_r = -17$ faint magnitude cutoff of our catalogue. For reference, we show also the approximate location of a few well-known systems, such as the Milky Way and M31 (both of which fall outside the plot), the Virgo cluster (Trentham & Hodgkin 2002), and three "fossil" groups: RX J1340.6+4018 (Jones et al. 2000), RX J1552.2+2013 (Mendes de Oliveira et al. 2006) and RX J1416.4+2315 (Cypriano et al. 2006). Magnitudes have been converted to the r-band using (Fukugita et al. 1995) when necessary. *Bottom panel:* Luminosity distribution of all red ($(g - r) > 0.95$) primaries (black solid histogram).The shaded magenta histogram indicate the subsample shown in the upper panel. These are the red *host* primaries having at least 10 satellites within r_{200}.

Figure 4. Number density profile of satellites within ~ 2 virial radii, computed after scaling the position of all satellites to the virial radius of the primary halo, and normalized at $r = r_{200}$. The contribution of *WSUB* and *NOSUB* satellites to the density profile is shown as well. Note that the majority of satellites near the center have had their parent halo stripped. The shape of the density profile is well approximated by an NFW profile with $c_{200} \sim 5.6$. This is slightly less concentrated than the "average" halo around these primaries, for which we estimate $\langle c_{200} \rangle \sim 8.1$. Both of these curves are shown in the figure, using the same normalization as for the satellites. Arrows indicate the radius containing half of the objects in each profile.

semianalytic model is able to reconcile the hierarchical growth of structure with the observed down-sizing of star formation in galaxies and the presence of "red and dead" galaxies at early epochs (Croton et al 2006, De Lucia et al 2006, Bower et al 2006).

The above interpretation suggests that the three "sequences" may be best appreciated by applying color cuts to the sample, since starburst galaxies will be bluer than average, while the opposite will be true for galaxies that have not formed stars recently. This expectation is largely borne out, as shown by the other three panels in Figure 1: galaxies bluer than $g - r = 0.65$ trace predominantly the "bright" sequence, whereas those redder than $g - r = 0.95$ largely trace the "underluminous sequence". The "main sequence" is nicely traced by galaxies of intermediate, less extreme, colors. We hasten to add that the color discrimination is not perfect, and that residual evidence for the "main sequence" is clearly apparent in both the red and blue panels of Figure 1.

The main conclusion from this discussion is that, at fixed luminosity, the virial mass depends strongly on color, and that a strict color selection criterion applied to primaries helps to tighten substantially the scaling between virial mass and luminosity (see e.g., Klypin & Prada 2007). As we discuss below, the large scatter that would result from blindly stacking primaries in luminosity bins would most likely obscure many of the underlying trends.

The prevalence of each of these sequences is a sensitive function of halo mass and galaxy luminosity. This is illustrated in Fig-
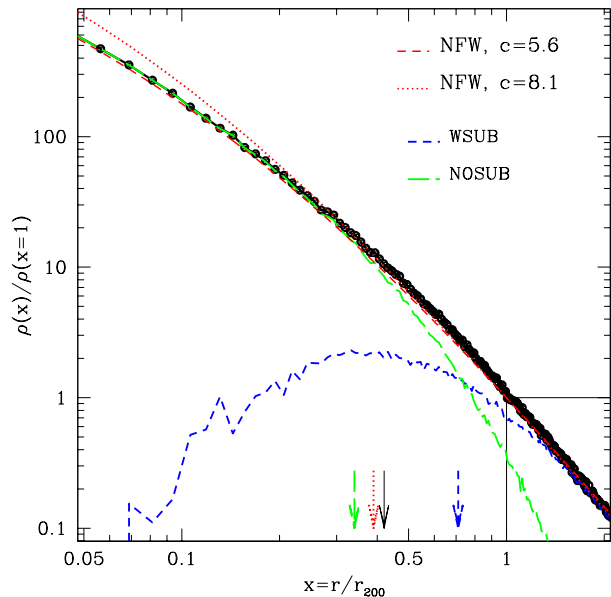
ure 2, where each panel shows, for several luminosity bins, the distribution of virial masses of galaxies in each of the three sequences. The sample is further split into *host* and *single* primaries, since, by definition, only the halos of *host* primaries are amenable to satellite dynamical studies.

Blue primaries are clearly in the minority amongst host galaxies, except at the brightest magnitudes, where they make a substantial ($\sim 29\%$) fraction of the brightest ($L > 10^{11} L_\odot$) primaries. Red galaxies, on the other hand, are reasonably well represented at all magnitudes, making up about $\sim 30\text{-}40\%$ of all primaries fainter than $10^{11} L_\odot$. The "main sequence" of primaries dominates at all but the brightest luminosities: intriguingly, only blue and red primaries make up the population of $L > 10^{11} L_\odot$ hosts. These are clearly very unusual objects, either the result of a recent starburst in a relatively low mass halo, or the result of growth by mergers but without star formation at the center of a very massive halo.

Single primaries show similar mass-color-luminosity trends as *hosts*, although galaxies with extremely red colors are less well represented, and the "main sequence" is more prevalent than amongst *hosts*. Interestingly, only blue *single* primaries in low mass halos populate the brightest luminosity bin ($L > 10^{11} L_\odot$): this is clearly the result of a major merger fueling a starburst of extreme but short-lived brightness.

At given luminosity, *single* primaries tend to have lower virial masses than *hosts*. This is expected, since more massive halos tend to have more of everything, including satellites, implying a small bias toward more massive halos in a sample selected to have at least one satellite. The effect is noticeable, as witnessed by the shift in
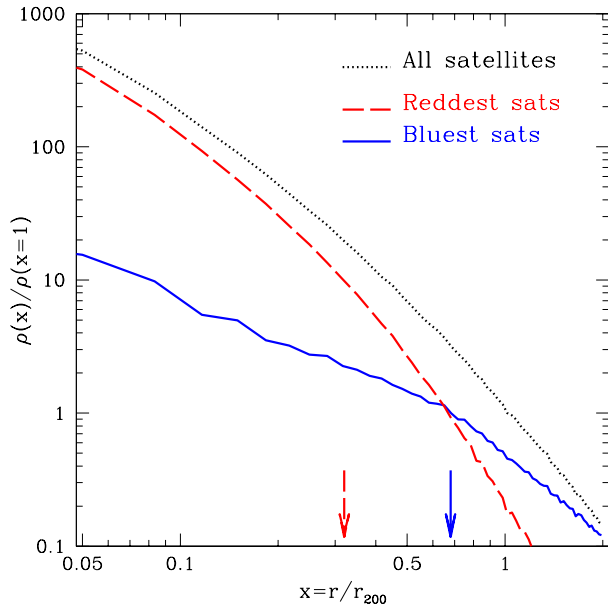
Figure 5. The color dependence of the satellite number density profile. The thick dotted line shows the profile corresponding to *all* satellites, as in Figure 4. The dashed (red) and solid (blue) curves show the contribution to the total profile of the reddest $((g - r) > 1.01)$ and bluest $((g - r) < 0.95)$ one-third of the satellites. Note that the reddest satellites are significantly more concentrated than the bluest ones. Arrows indicate the radius enclosing half of the satellites in each subsample.

the position of the green histogram in corresponding panels of the *single* and *host* distributions shown in Figure 2. As expected from the argument below, it is largest in the lowest luminosity bins (i.e., $L < 10^{10.4} L_{\odot}$), where it amounts to a shift by a factor of ~ 2 in the average mass of galaxies in the "main" sequence.

3.2 Application to "fossil groups"

As is clear from Figures 1 and 2, our primary selection criteria select a number of systems in fairly massive halos, 10^{13}-$10^{15} M_{\odot}$, a range usually associated with galaxy groups and poor clusters rather than isolated galaxies. These are, indeed, systems of galaxies which, by chance, have evolved a gap of at least two magnitudes between the brightest and second brightest galaxy, and therefore are included in our sample. These systems are not rare; according to Table 1, the brightest galaxy of about $\sim 10\%$ of all halos in the range 10^{13}-$10^{15} M_{\odot}$ is a primary according to our definition.

The presence of these systems in our sample has the potential of biasing our satellite velocities toward large values, and therefore one must be careful to take this into account in the analysis. We shall return to this issue below (§ 3.6); but we note here that these are the analogs of "fossil groups", systems of galaxies which are unusually X-ray bright (and massive) for their optical richness. "Fossil" groups or clusters are defined, just like our primaries, as systems where a large (> 2) magnitude gap exists between the brightest and second-brightest galaxy.

Although the statistics of these objects are still fairly poorly known, their unusual properties have attracted attention from observers and theorists alike, and there has been speculation that the abundance of these systems might be difficult to reproduce in the ΛCDM cosmogony (D'Onghia & Lake 2004; D'Onghia et al.

2005; Milosavljević et al. 2006; Sommer-Larsen 2006). Subsequent work has shown, however, that the predicted abundance of "fossil" systems is in reasonable agreement with the still rather uncertain observational constraints (see, e.g. D'Onghia et al. 2007; van den Bosch et al. 2007). Worries remain that the atypical luminosity function of known 'fossil' systems may be difficult to reconcile with the substructure function of ΛCDM halos (D'Onghia et al. 2007), but we emphasize that *only three* "fossil" groups have published luminosity functions. This, however, should change soon, as available X-ray data are systematically surveyed for the presence of "fossil" groups, and as imaging and spectroscopic surveys provide secure luminosity functions for a growing number of "fossil" groups.

Our intention here is to characterize the abundance and luminosity function of "fossil"-like systems in our galaxy catalogue in order to guide the interpretation of future observational constraints. As stated above, these objects are not rare, since up to one in ten of the most massive halos may be regarded as a "fossil" system according to the above definitions (see Table 1). These systems are not rare amongst bright galaxies either, as shown in Table 2; approximately 22% of galaxies brighter than $5 \times 10^{10} L_{\odot}$ live in a "fossil"-like environment. "fossil"-like systems are more prevalent amongst fainter galaxies, which tend to inhabit lower mass halos, where large magnitude gaps between the two brightest galaxy members are common (e.g., the Milky Way is the "ultimate fossil group").

This gives a total number density of $8.1 \times 10^{-6} h^3$ Mpc^{-3} for "fossil" systems in halos exceeding $10^{13} h^{-1} M_{\odot}$, or $8.3 \times 10^{-5} h^3$ Mpc^{-3} for fossil groups whose brightest galaxy exceeds $5 \times 10^{10} h^{-2} L_{\odot}$. This actually exceeds the (still rather uncertain) observational estimates of $\sim 5 \times 10^{-7} - 2 \times 10^{-6} h^3$ Mpc^{-3} (Jones et al. 2003; Vikhlinin et al. 1999; Romer et al. 2000) for groups with X-ray luminosities $\geqslant 10^{43} h_{50}^{-2}$ erg s^{-1}. We note, however, that only about 10 fossil groups are actually known, and that this may very well be an underestimate. Our preliminary conclusion is that the semianalytic approach has no difficulty accounting for the abundance of groups with such a strong distinction between brightest and second-brightest galaxy.

A further test concerns the actual luminosity distribution of galaxies in the groups. In a recent paper, D'Onghia et al (2007) argue, on the basis of N-body simulations, that "fossil" groups present a challenge to the ΛCDM scenario, since few cold dark matter halos are as deficient in substructure as "fossil" groups. This suggestion is based on the analysis of simulations that follow solely the dark matter component, so it is important to check the predictions of models that actually follow the formation of the galaxies.

We adopt a simple measure of the shape of the luminosity distribution of galaxies in a "fossil" group, namely the magnitude difference between the brightest and tenth brightest galaxy member, ΔM_{10}. This is shown as a function of primary luminosity in the top panel of Figure 3. A typical cluster with a well populated Schechter-like luminosity distribution, such as Virgo, has $\Delta M_{10} \sim 2$ (Trentham & Hodgkin 2002). Individual galaxies, such as the Milky Way or M31, have a much larger percentage of the total light concentrated in a single object, and as a result their ΔM_{10} differ markedly from Virgo; we find $\Delta M_{10} = 9$ and 11 for the Milky Way and M31, respectively (Mateo 1998). Fossil groups have intermediate values of ΔM_{10}; for the three groups with published luminosity functions, the values span the range from ~ 3 to ~ 5 (Jones et al. 2000; Mendes de Oliveira et al. 2006; Cypriano et al. 2006).

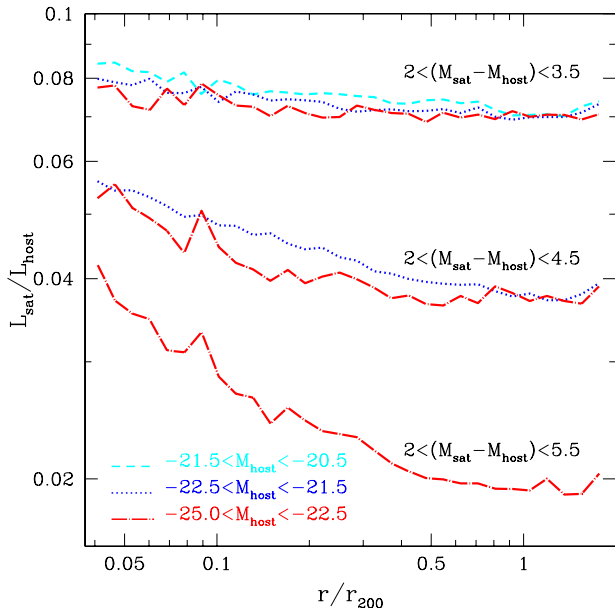These values are not unusual in our catalogue of isolated pri-

Figure 6. The average satellite luminosity (expressed in units of $L_{\rm host}$) is shown as a function of radius for various primary luminosity bins. Because of our faint magnitude cutoff ($M_r = -17$), we consider a different magnitude range for satellites, depending on the brightness of the host. The three dot-dashed lines correspond to primaries brighter than $10^{10.8}\, L_{\odot}$ ($M_r \lesssim -22.5$). Note that when considering the full magnitude range resolved in the *MS*, ($2 < M_{\rm sat} - M_{\rm host} < 5.5$) a strong luminosity segregation is clearly present: the average brightness of satellites decreases by a factor of ~ 2 from the center out to the virial radius. As expected, the magnitude of the effect decreases as the magnitude range narrows when considering fainter hosts. Once this effect is taken into account, the satellite luminosity segregation seems to be roughly independent of host brightness.

maries, where ΔM_{10} is a strong function of the primary luminosity, approaching ~ 2 (the minimum possible value given our isolation criterion) for the brightest primaries, but increasing rapidly with decreasing luminosity. As shown in the top panel of Figure 3, there is also a large scatter in ΔM_{10}; at $L \sim 10^{11} L_{\odot}$ we find values that go from ~ 3 to ~ 6, spanning the range observed in fossil groups. It would clearly be difficult to argue on the basis of this evidence that there is a substantial discrepancy between ΛCDM predictions and the observations of "fossil" groups. Further data are needed to clarify this issue further.

3.3   Satellite density profile

The solid circles in Figure 4 show the number density profile of satellites, computed after rescaling the position of each satellite to the virial radius of the host and stacking the full sample. The large number of satellites in our catalogue makes the statistical error in the profile negligible; bootstrap error bars are smaller than the size of each symbol.

The shape of the satellite density profile is well described by the NFW (Navarro, Frenk & White 1996, 1997) formula, with $c_{200} = 5.6$. This result is rather insensitive to halo mass or luminosity, for example, splitting the sample of primaries in two by halo mass results in $c = 5.6 \pm 0.3$ and 6.2 ± 0.5 for the high and

low mass sample, respectively. A similar split in luminosity yields $c = 6.2 \pm 0.6$ and $c = 5.5 \pm 0.4$, respectively.

Satellites are slightly less concentrated than the host dark matter halos. The average host dark halo concentration may be found by averaging the concentrations of host halos, estimated from the mass-concentration relation of Fausti-Neto et al (in preparation):

$$\log(c_{200}) = 2.1 - 0.1 \log(M_{200}/(M_{\odot}/h)^{-1}), \qquad (1)$$

and taking into account the lognormal dispersion $\sigma(\log(c_{200})) = 0.10$. We find an average concentration of $\langle c_{200} \rangle = 8.1$.

These two NFW profiles are plotted in Figure 4, showing that the difference is not large. For example, the half mass radius of the average dark halo is $0.39\, r_{200}$, which is very similar to the radius that contains half of the stacked satellites, $0.42\, r_{200}$. We conclude that satellites are a relatively unbiased tracer of the dark mass distribution within the virial radius of a halo, at least for this model of galaxy formation and evolution.

In a recent paper, Chen et al. (2006) study the radial projected distribution of satellite galaxies in the SDSS. These authors find that the projected satellite number density profile is well fitted by a power law: $\Sigma(R) \propto R^{\alpha}$, with $\alpha = -1.7 \pm 0.1$. In order to approximately mimic the selection criteria applied by Chen et al., we have projected all galaxies in our catalogue within $1\ h^{-1}$Mpc around each isolated primary, considering as "satellites" those within projected distances $\Delta R < 500\ h^{-1}$ kpc and line-of-sight velocities $\Delta V_{los} < 500$ km/s (notice that from our definition of isolated galaxies, all "satellites" are at least two magnitude fainter than the primary). We find $\alpha = -1.55 \pm 0.08$ in the distance range $26 < R < 500\, h^{-1}$kpc, which is consistent with the results of Chen et al within the quoted errors.

3.3.1   Dependence on satellite color

Although the satellite population as a whole traces the dark mass reasonably well, there is a strong dependence on satellite color. This is shown in Figure 5, where the profiles of the reddest ($(g - r) > 1.01$, red dashed line) and bluest ($(g - r) < 0.95$, solid blue line) one-third of satellites is compared with the overall profile presented in Figure 4. Red satellites are clearly much more centrally concentrated than blue ones: half of the red sample is contained within $0.32\, r_{200}$, a radius that climbs to $0.71\, r_{200}$ for the bluest one-third of satellites.

This difference in concentration may be traced to the assumption in the semianalytic treatment that a satellite loses its reservoir of hot gas (the future fuel for star formation) once it is accreted into a larger structure. Thus star formation in satellites declines quickly after accretion: the earlier a satellite was accreted the older (and redder) its stellar population will be. Early-accreting satellites have smaller turnaround radii and are likely to orbit closer to the center than late accreting ones, resulting in the trend shown in Figure 5.

A trend of similar origin is shown also by the bottom two curves in Figure 4, which show the contribution to the satellite density profile from satellites that have preserved (*WSUB*) or lost (*NO-SUB*) their parent dark halos. Early accreting satellites are more likely to have been more affected by tides and to have lost their parent halos, leading to the spatial segregation between *WSUB* and *NOSUB* satellites seen here. This figure also shows clearly the importance of tracking satellites in dark matter-only simulations even after their parent halos have been disrupted in the tidal field of the primary: *NOSUB* satellites are crucial to the satellite profile in the inner regions of the primary.
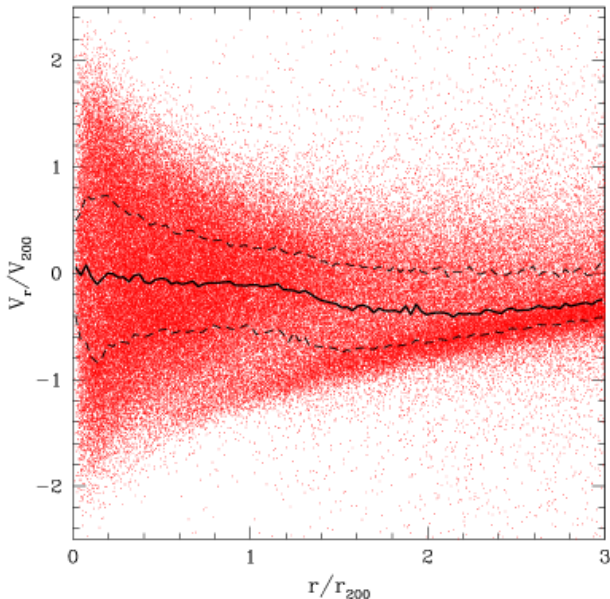
center on a shorter timescale. It should be possible to contrast this result against observation. However, a note of caution about this interpretation is in order, recalling the results of Figure 4. Since most satellites, especially those near the center, have lost their parent halo, their present-day location is being traced by a single dark matter particle, and their survival depends directly on the semianalytic model assumptions about dynamical friction. As such, the luminosity segregation shown in Figure 6 is likely to be model-dependent.

3.4 Satellite Velocities

3.4.1 Radial velocities

Figure 7 shows the radial velocities of all satellites in our sample as a function of their distance to the primary, after rescaling to the virial quantities of the host halo. The solid line traces the median satellite velocity in radial bins; the dashed lines the 25% and 75% of the distribution, respectively. Note that the median velocity within r_{200} is constant and consistent with zero, as expected from a relaxed population in equilibrium.

Outside r_{200}, negative velocities are more prevalent, as satellites on their first approach to the primary start to dominate. These "first-infall" satellites delineate the negative velocity boundary at all radii, forming a sequence that becomes fairly obvious outside $\sim 0.5\,r_{200}$ in Figure 7. The velocity along this sequence decreases outward, and approaches zero at $r \sim 3\,r_{200}$, the approximate location of the turnaround radius according to the simple secondary infall model (see Bertschinger 1985; White et al. 1993; Navarro & White 1993).

The "first-infall" sequence is an interesting feature of the radial velocity distribution, one whose detection may be used to yield a direct estimate of the mass of the host halo. This is the rationale of a number of studies that attempt to pin down the location of the turnaround radius in the outskirts of galaxy groups and clusters by looking at "caustics" in the velocity distribution (Diaferio & Geller 1997; Diaferio 1999; Geller et al. 1999; Biviano & Girardi 2003; Rines et al. 2003; Diaferio et al. 2005). Although some progress has been made on this issue, the observational evidence remains elusive and its interpretation controversial (Reisenegger et al. 2000; Drinkwater et al. 2001; Mahdavi et al. 2005; Mohayaee et al. 2006; Gavazzi et al. 2006).

Figure 7 offers a possible explanation for these findings: satellites on first approach make up a relatively small fraction of systems populating the outskirts of the halo. We investigate this quantitatively in Figure 8, where we show the satellite radial velocity distribution as a function of radius, $x = r/r_{200}$, normalized to the virial radius.

Satellites within the virial radius have an approximately Gaussian velocity distribution with dispersion that declines with radius. Interestingly, the radial velocity dispersion in the inner regions is comparable to the virial velocity of the halo, $\sigma_r \sim 0.96\,V_{200}$. This result has been used by Sales et al (2007a) to argue that the relatively low velocity dispersion of Galactic satellites implies a fairly low mass for the Milky Way halo ($V_{200}^{MW} \sim 110$ km/s, see that paper for further details). The velocity dispersion declines outward: the best fitting Gaussian for satellites with $0.5 < x < 1$ is $\sigma_r \sim 0.7\,V_{200}$.

Beyond the virial radius, the radial velocity distribution becomes clearly asymmetric, with an excess of satellites with negative radial velocities. As mentioned above, this is a result of the increasing importance of satellites on their first approach to the host halo.

Figure 7. The radial velocity of all satellites in our sample as a function of radius, both scaled to the virial values of the host halo. The solid curve shows the median of the distribution, while dashed lines outline the 25% and 75% percentiles of the distribution as a function of radius. The velocity dispersion decreases out to the virial radius beyond which it remains approximately constant. A "first infall" sequence of negative radial velocities is clearly defined outside $\sim 0.5\,r_{200}$. Satellites with very high radial velocities (sometimes exceeding $\sim 3\,V_{200}$) are present, especially at large radii. This is a result of some primaries lying in the periphery of much larger structures, such as galaxy clusters; the large velocities are those of cluster members typically unrelated to the primary.

3.3.2 Dependence on satellite brightness

Figure 6 explores the luminosity segregation of satellites and its dependence on primary luminosity. The faint magnitude cutoff of our catalogue implies that, in order to compare meaningfully primaries of different brightness, satellites must be selected within a definite magnitude range. Satellites can only have absolute magnitudes between the cutoff at $M_r = -17$ and $M_{\rm host} + 2$, so that fainter primaries have, by construction, satellites that span a narrower magnitude range.

The three (red) dot-dashed curves in Figure 6 indicate the radial dependence of the average satellite luminosity (in units of the host's) for the brightest hosts ($L_r > 10^{10.8}\,L_\odot$; $M_r < -22.5$). When all satellites are considered (i.e., in the magnitude range $2 < M_{\rm sat} - M_{\rm host} < 5.5$; bottom curve in Figure 6) a significant radial trend is seen: the average satellite luminosity drops by a factor of ~ 2 from the center out to the virial radius. The trend is, as expected, more difficult to detect when a narrower range in satellite brightnesses is imposed (upper two curves). Such a narrower range is needed when considering fainter primaries, for which results are shown by the dashed and dotted curves in Figure 6. Once this is taken into account the luminosity segregation we find seems to be independent of the brightness of the primary.

The luminosity segregation shown in Figure 6 is most likely due to the effects of dynamical friction, which operate faster on more massive/more luminous satellites, bringing them closer to the

We have chosen to quantify this with a double Gaussian fit: one of zero mean velocity and dispersion fit to the distribution of *positive* radial velocities, and a second one whose dispersion and mean are chosen so that the sum of the two Gaussians match best the whole distribution. The two Gaussian fits are shown with dashed lines in Figure 8, and we shall hereafter refer to them, for short, as the "zero mean velocity" component (*zmv*) and the "infall" component (*inf*). Values quoted in each panel of figure 8 indicate the best-fit Gaussian parameters to the *total* distribution[4]. In contrast with the results of Prada et al. (2006) and Power (2006), the infall patern is insensitive to halo mass; we find a non-negligible population of first-infall satellites around low and high-mass halos in our catalogue.

As expected, the mean infall velocity decreases outward, from $\bar{V}_r \sim -0.85\,V_{200}$ at $1 < x < 1.5$ to $\bar{V}_r \sim -0.4\,V_{200}$ at $2.5 < x < 3$, and consistent with a turnaround radius located just outside $\sim 3\,r_{200}$. Interestingly, the velocity dispersion of infalling satellites amounts to about 15% and 25% of the virial velocity of the host halo, about a factor of two to three colder than the rest of the population. The prevalence of the first-infall population increases outward: it makes up 15%, 25%, 36%, and 40% of all satellites in each of the four $x > 1$ bins shown in Figure 8, respectively. These results may be used to improve algorithms intended to detect infalling galaxies in the regions surrounding groups and clusters.

3.4.2 Tangential velocities

In order to complete our characterization of satellite velocities we show in Figure 9 the distribution of the tangential velocity components, binned by distance just as in Figure 8. The spherical components are measured in a reference frame where the z-axis is chosen to coincide with the angular momentum of the host halo, so that V_ϕ carries information about a satellite's sense of rotation relative to the host.

Within the virial radius the dispersion in V_ϕ and V_θ is substantially lower than the radial dispersion, and there are also hints of significant departures from Gaussianity. There is, for example, an excess of satellites that co-rotate with the host (i.e., $V_\phi > 0$); also, the V_θ distribution is platykurtic; i.e., it is more centrally peaked and has broader wings than a Gaussian. Such departures from Gaussianity are more pronounced for satellites outside the virial radius.

The long- and short-dashed curves in Figure 9 show the contribution to the total velocity distribution of the "infall" and "zero-mean velocity" components discussed in § 3.4.1. This is done by assigning satellites probabilistically to each of the two components, according to the Gaussian decomposition shown in Figure 8. Interestingly, the V_θ distribution, which is *not* well approximated by a Gaussian, is found to be the result of adding the nearly Gaussian distributions corresponding to the "infall" and the "zero-mean velocity" components. Note, as well, that even *inside* r_{200} the V_θ distribution differs slightly from a Gaussian. This is most likely due to the presence of infalling satellites within the virial radius. Although they are difficult to pick up in radial velocity, there are apparently

[4] We will use $\bar{V}_i$ and σ_i to indicate the mean and dispersion of the i-component velocity distribution, where $i = r, \theta, \phi$. The skewness ξ is defined as $\frac{\Sigma(V_i - \bar{V}_i)^3}{(N-1)\sigma_i^3}$ and the kurtosis $\kappa = \frac{\Sigma(V_i - \bar{V}_i)^4}{(N-1)\sigma_i^4} - 3$
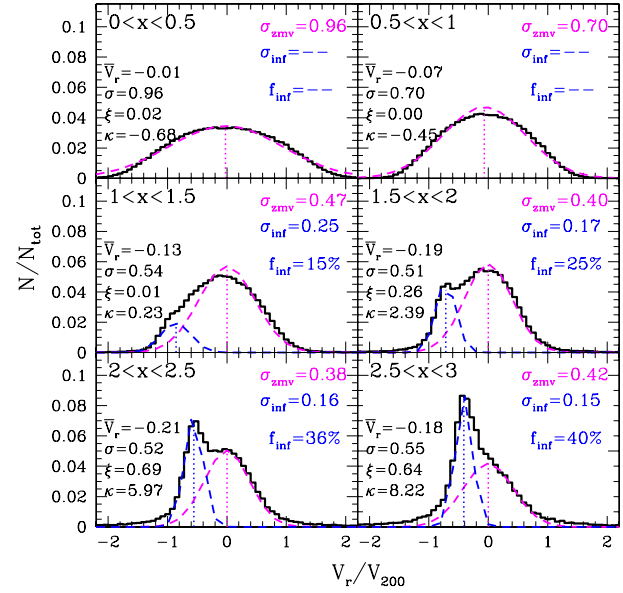

Figure 8. Distribution of satellite radial velocities, in bins of different distance to the primary. We consider only *central* hosts here in order to minimize the contribution of velocity interlopers. The radial range considered in each panel is labeled by the range in $x = r/r_{200}$ used. Dashed lines show Gaussian fits to the profiles: *two* Gaussians are used when the distribution shows a strong asymmetry between negative and positive radial velocities. One of the Gaussians (the *zmv* component) is assumed to have zero mean velocity and to match the distribution of positive radial velocities; the parameters of the second one (the *inf* component) are then fit so as to match the whole distribution. The fit parameters (mean V_r, dispersion σ_r, skewness ξ and kurtosis κ) are given in Table 3 as well as quoted in each panel.

enough of them to modify the V_θ distribution from Gaussian to platykurtic.

As may be seen from the right-hand panel of Figure 9, the V_ϕ distribution of the "infall" component is approximately Gaussian as well, and shows only a weak excess of satellites co-rotating with the host. The "zero-mean velocity" component, on the other hand, shows a much more pronounced asymmetry and a broader dispersion. It is not clear at this point what causes this difference, but we plan to follow it up in future work. In all cases, the dispersion in the "infall" component is significantly lower than in the ZMV component. Table 3 lists a summary of the fit parameters for all these velocity components.

3.4.3 Velocity anisotropy

The velocity dispersion of the various spherical components declines gradually with radius, as shown in Figure 10. The biggest decline is seen for the radial velocity dispersion, which drops by almost a factor of two from the center out to the virial radius. The dispersion in the other components drops with radius at a different rate, leading to an anisotropy profile that increases from the center outwards, reaches a maximum of $\beta_{\max} \sim 0.5$ at $r \sim 0.2\,r_{200}$ and declines to become almost isotropic $\beta \sim 0$ just outside the virial radius.

The radial dependence of the anisotropy is a reflection of the increasing importance of the first-infall population at larger radii. Because it is on its first approach, the *inf* population is "stretched" along the radial direction and has therefore a smaller radial velocity
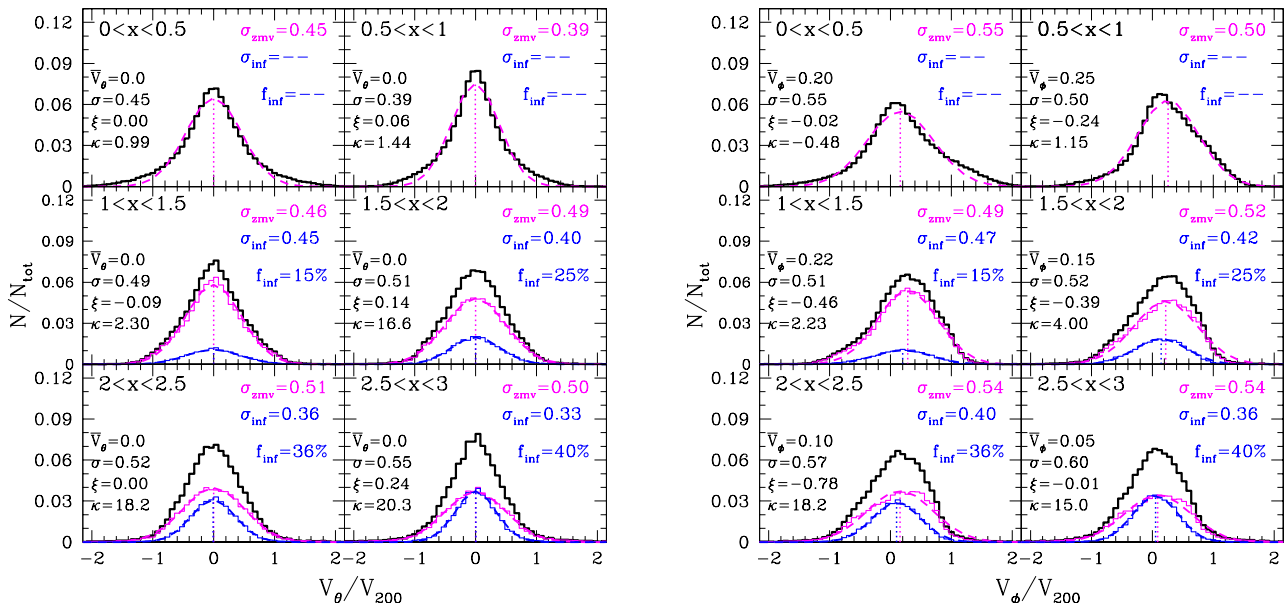
Figure 9. Distribution of the tangential spherical components of the satellite velocities, V_θ and V_ϕ, shown in various distance bins, $x = r/r_{200}$, as labelled in each panel. We have split the sample in two components, an "infall" component (*inf*, magenta long-dashed lines) and a "zero-mean velocity" component (*zmv*, solid black line), using the double Gaussian fits to the radial velocity distribution of Figure 8 to assign probabilistically satellites to each. Dotted curves are Gaussian fits to each of these distributions. Parameters (mean, dispersion σ, skewness ξ and kurtosis κ, are quoted in each panel and in Table 3.

dispersion at any given radius, compared with its tangential dispersion (compare, e.g., the radial and tangential dispersions for the *inf* population in Figures 8 and 9). As the prevalence of this component increases outwards, it brings down the radial bias characteristic of the inner regions, leading to a decline of the anisotropy in the outskirts of the system. In support of this interpretation, we note that the anisotropy of *WSUB* satellites differs strongly from that of *NOSUB* satellites (Figure 10). The former still retain their parent halos; are therefore more likely to have been accreted into the system more recently; and have velocities that are more isotropic than the rest.

Figure 10 shows that the satellite velocity dispersion at the virial radius is about 40% its maximum value in the inner regions. This decline is in agreement with that expected for NFW halos and can be successfully recovered from observational samples when contamination from interlopers is properly accounted for. Although early studies suggested a nearly flat satellite velocity dispersion profiles favouring isothermal models for host halos (McKay et al. 2002; Brainerd & Specian 2003), subsequent analysis suggested that it might be due to poor removal of background and foreground interlopers. Prada et al. (2003) studied the dynamic of satellite galaxies in the SDSS removing interlopers from their samples fitting a "Gaussian + constant" function to the satellite velocity distributions. These authors find that the projected velocity dispersion of *true* satellites drops to $\sim 40 - 60\%$ its maximum value at a projected distance of $\Delta R \sim 300 h^{-1}$kpc from the primary. The analysis of satellites in the 2dFGRS catalogue also show a declining σ profile after interloper remotion, although the measured drop in the velocity dispersion with distance is somewhat weaker (Brainerd 2004a). The satellite galaxy kinematics in the Millennium Simulation appears broadly consistent with these observational results.

3.5 Halo mass profile from satellite dynamics

Once the spatial distribution and the kinematics of the satellite population have been characterized, we may use them to constrain the shape of the host halo mass profile. Assuming spherical symmetry, equilibrium, and that satellites are massless tracers of the potential, Jeans' equations link the potential with the velocity dispersion and density profiles of the satellites. Expressed in terms of a circular velocity, we have:

$$V_c^2(r) = -\sigma_r^2 \left(\frac{d \ln \rho}{d \ln r} + \frac{d \ln \sigma_r^2}{d \ln r} + 2\beta \right), \qquad (2)$$

where the terms in the right hand side may be estimated from the results in the preceding discussion, and are summarized in the top panel of Figure 11.

The implied circular velocity profile for the *average* halo populated by the satellites is shown in the bottom panel of Figure 11. This V_c profile has several of the same characteristics of the NFW profile: it rises to a maximum and then drops near the virial radius. The maximum circular velocity implied is $V_{\max} \sim 1.25 \, V_{200}$, and occurs at $r_{\max} \sim 0.3 \, r_{200}$, which corresponds to a concentration of $c_{200} \sim 7$. We note that this is higher than the concentration (~ 5.6) derived from fitting an NFW profile to the number density of satellites (Figure 4), and is closer to the *average* concentration of $\langle c \rangle \sim 8.1$ found for the host halos in the *MS* (see § 3.3). In spite of these differences, it is remarkable that satellites are overall reasonably good tracers of the dark mass profile. These similarities have also been reported in N-body/gasdynamical simulations by Sales et al (2007a), and augur well for studies of the mass profile of galactic halos based on satellite data.
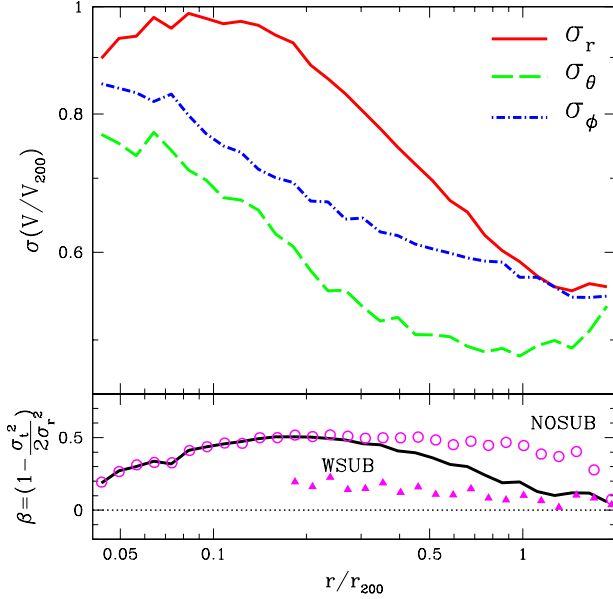
Figure 10. *Upper panel:* Velocity dispersion profile of central host satellites in spherical coordinates, where the polar z axis is chosen to coincide with the direction of the host angular momentum. *Lower panel:* The corresponding anisotropy parameter, $\beta = 1 - \sigma_t^2/2\sigma_r^2$, where $\sigma_t^2 = \sigma_\theta^2 + \sigma_\phi^2$. We distinguish in the bottom panel the contribution of satellites that have preserved their parent dark matter halo (*WSUB*, filled triangles) and those that have not (*NOSUB*, open circles).

3.6   Primary luminosity vs satellite velocity dispersion

The velocity dispersion of satellites is one of the prime tools used to investigate the mass of dark halos surrounding isolated galaxies and its dependence on luminosity. In hierarchical formation scenarios like ΛCDM, velocities vary with mass according to the virial definitions discussed in the footnote to § 2.3.2, which imply that mass scales with velocity like $M_{200} \propto V_{200}^3$.

Due to the small number of satellites surrounding each primary, it is necessary to combine them in some way in order to beat small-number statistics. One obvious choice is to bin primaries in a narrow luminosity range, stack their satellites, compute their velocity dispersion, and see how the dispersion varies as a function of the luminosity of the primary.

If satellite velocities are an unbiased tracer of the virial velocity, and luminosity is a reasonable proxy for mass, then one may expect $L \propto \sigma^3$. The former assumption appears to be borne out by the analysis presented above, but the latter one is afflicted by the large scatter in the mass-luminosity relation discussed in § 3.1. How does this affect the scaling between primary luminosity and satellite velocity dispersion?

We show this in Figure 12, where hosts are binned according to their r-band luminosity, and the one-dimensional velocity dispersion is computed for each bin after stacking all of their satellites. In each panel, the solid circles show the result of this procedure including all satellites of hosts satisfying the condition expressed in the label. The short-dashed (blue), long dashed (green) and dot-dashed (red) curves correspond to selecting primaries according to the color cuts adopted in Figure 1. The dotted lines indicate, for reference, the $L \propto \sigma^3$ and $L \propto \sigma^2$ scalings.

When considering all primaries (top-left panel), the L-σ relation is poorly fit by a power law, bending from approximately
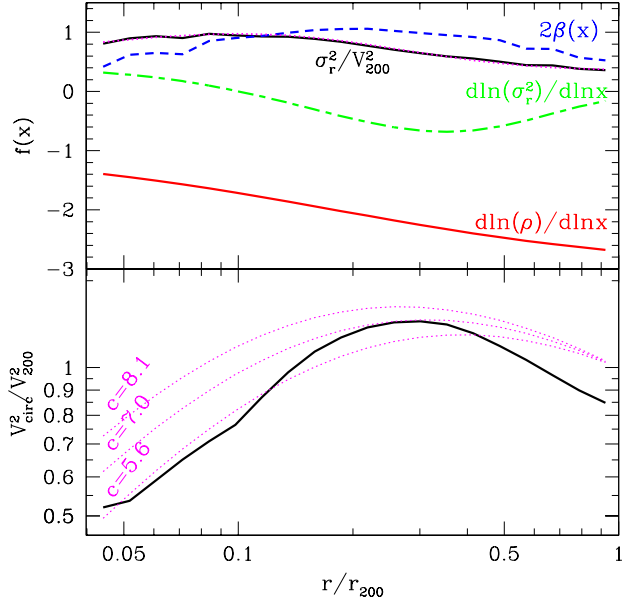

Figure 11. *Top:* Terms in the right-hand side of Jeans' equation relating satellite dynamics and the halo mass profile (eq. 2). The dotted line shows a fit to $\sigma_r(r)$ of the form: $\sigma_r/V_{200} = \sigma_0 + (x/x_0) \exp(-(x/x_0)^\alpha)$, with $x = r/r_{200}$. Best-fitting dimensionless parameters are: $x_0 = 0.068$, $\alpha = 3/4$ and $\sigma_0 = 0.6$. *Bottom:* Solid line shows the average circular velocity profile of the potential sampled by the satellites, as derived from applying Jeans' equation. Note that the circular velocity implied by the satellite population rises to a maximum before dropping near the virial radius. The maximum circular velocity implied is consistent with an NFW profile with $c_{200} \approx 7$. This is in reasonable agreement with the average concentration ($\langle c \rangle \approx 8.1$) of host halos inhabited by satellites, and is higher than the concentration derived from the satellite density profile in Figure 4.

$L \propto \sigma^2$ at faint luminosities to a substantially shallower scaling for $L > 5 \times 10^{10} L_\odot$. A similar departure of the $L - \sigma$ relation from a simple power-law scaling has been reported and discussed previously by van den Bosch et al. (2004). This is quite different from the naive scaling mentioned above for hierarchical models, and is largely due to the large scatter in the halo mass-luminosity relation shown in Figure 1. The presence of some very massive halos at all luminosities, together with their growing importance with increasing luminosity bend the relation off the natural $L \propto \sigma^3$ scaling. At $\sim 5 \times 10^{10} L_\odot$ the prevalence of such massive objects increases and the relation becomes even shallower.

Restricting primaries by color helps; for example, for blue hosts $((g-r) < 0.65)$ we obtain a $L \propto \sigma^3$ relation that holds over the whole luminosity range. However, color cuts work less well for redder primaries: for $0.65 < (g-r) < 0.95$ hosts we recover the $L \propto \sigma^3$ relation at faint luminosities, although for galaxies brighter than $\sim 6 \times 10^{10} L_\odot$ the scaling becomes again much shallower as a result of the growing importance of massive halos with underluminous central galaxies. The same applies to the primaries with the reddest colors, although the change in the slope occurs at fainter luminosities ($\sim 4 \times 10^{10} L_\odot$). Selecting by color alone is thus not enough to ensure a sample of primaries with a well-defined power-law scaling between luminosity and velocity dispersion.
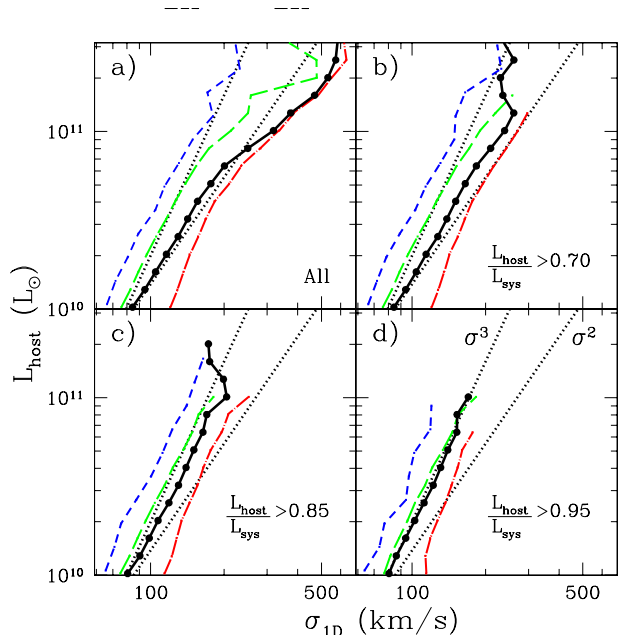
Figure 12. Velocity dispersion of satellites around isolated galaxies binned by r-band luminosity. Dispersions are computed after stacking all satellites within the virial radius of the host of each galaxy in the bin. Solid connected circles show the results for all satellites of primaries satisfying the criterion indicated by the label in each panel. Short-dashed (blue), long-dashed (green) and dot-dashed (red) curves correspond to primaries selected according to the color cuts chosen in Figure 1. Dotted lines indicate $L \propto \sigma^3$ and $L \propto \sigma^2$ scalings, to ease the comparison from panel to panel. Panels differ in the sample of primaries used. The importance of the primary within its own virial radius distinguishes these samples, as given by $L_{\rm host}/L_{\rm sys}$, where $L_{\rm sys}$ is the total luminosity of galaxies within the virial radius.
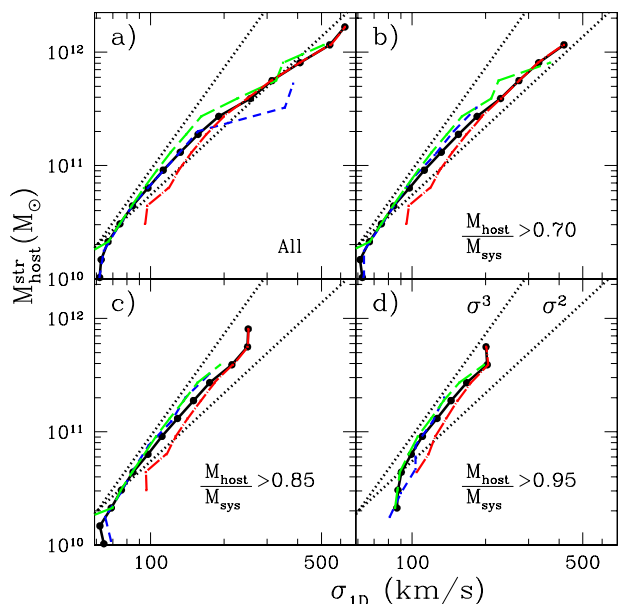

Figure 13. Same as figure 12, but considering stellar masses rather than r-band luminosities. Cuts applied on $M_{\rm host}/M_{\rm sys}$ refer also to the mass in stars.

One way of eliminating underluminous primaries within very massive halos from our sample is to consider the richness of their surroundings. Massive halos will typically host a large number of galaxies and in such systems, despite our isolation criteria, which ensures the dominance of the central galaxy, the other members may contribute a significant fraction of the total luminosity. This is shown in the other three panels of Figure 12, where we consider only primaries making up more than, respectively, 70%, 85%, and 95% of the total combined luminosity of galaxies within the host halo, $L_{\rm sys}$. The stricter the criteria for selecting the primaries the nearer the scaling is to the "natural" $L \propto \sigma^3$ relation. Selecting truly isolated galaxies thus requires more than just imposing a magnitude gap, but also a color cut and a conscientious survey of the surroundings to weed out fossil groups and poor clusters from the sample which may unduly bias the L-σ scaling. Alternatively, one may try and eliminate from the analysis the brightest galaxies, where the contamination by "fossil" systems is worse. This is the approach adopted by Prada et al. (2003), who show that the "natural" scaling may also be recovered in that case.

Despite the pruning of the sample, the dependence of the satellite velocity dispersion on the color of the primary remains. For our strictest isolation criterion, $L_{\rm host} > 0.95 \, L_{\rm sys}$, the velocity dispersion of satellites of red galaxies is $\sim 55\%$ higher than that of blue galaxies of given luminosity. This is reminiscent of the observations of Brainerd T. (2004a,b) in the 2dFGRS who found larger velocity dispersion in satellites associated to early-type (red) primaries than satellites of late-type (blue) hosts.

This effect is due largely to the different stellar mass-to-light ratios of galaxies of different colors. Indeed, as shown in Figure 13, the shift in velocity dispersion between primaries of different color basically disappears when *stellar masses* are considered instead of r-band luminosities. Using, whenever possible, stellar mass estimates rather than luminosity in order to bin galaxies is likely to give more robust results. Combining this with a strict isolation criterion that evaluates not only the luminosity gap between brightest and second-brightest galaxy but also the richness of the surrounding field appears essential in order to avoid biases and to recover the natural scaling expected from hierarchical structure formation scenarios.

3.7 Spatial anisotropies and the Holmberg effect

An issue that has drawn recurring attention over time is whether the spatial distribution of satellites around primaries has anisotropies of particular significance. For example, the brightest satellites around the Milky Way seem to align on a plane perpendicular to the disk of the Galaxy (Lynden-Bell 1982; Majewski 1994; Kroupa et al. 2005; Libeskind et al. 2005), and a similar result seems to apply to at least some of the satellites of the Andromeda galaxy (Koch & Grebel 2006; Metz et al. 2007). The small number of satellites involved in these analyses precludes robust conclusions to be drawn on the basis of the Local Group (Zentner et al. 2005), but it is intriguing that both Holmberg (1969) and Zaritsky et al. (1997b) find a similar effect in their samples of satellites of spiral galaxies.

The advent of large datasets, mostly from the SDSS, has allowed the issue to be revisited, and the latest work suggests that satellites of isolated spirals tend to distribute themselves preferentially along the direction of the disk: the *opposite* of the effect claimed by Holmberg and present in the Milky Way (Brainerd 2005; Azzaro et al. 2006; Yang et al. 2006; Agustsson & Brainerd 2007). One recent paper (Sales & Lambas 2004) argued that satel-

lites in the 2dfGRS actually follow Holmberg's suggestion, but this was in error due apparently to ambiguities in the way position angles are defined in the 2dfGRS database, and has now been resolved (Yang et al. 2006).

The anti-Holmberg effect is due to misalignment between the angular momentum and the triaxial structure of the host halos. A long literature has now established dark matter halos to be triaxial objects, with a preference for nearly prolate shapes, and whose angular momentum is perpendicular to the major axis of the halo (Frenk et al. 1988; Bullock et al. 2001; Bullock 2002; Jing & Suto 2002; Bailin & Steinmetz 2005; Hopkins et al. 2005; Bett et al. 2007). If satellites trace the shape of the dark matter halo and if the spin of the central galaxy disks preserves the direction of the halo angular momentum, then this would explain the scarcity of satellites near the rotation axis of the disk.

We examine this in Figure 14, where the anisotropy in the spatial distribution of satellites around primaries is measured by the distribution of the cosine of the polar angle (measured from the angular momentum axis of the SUBFIND subhalo centred on the host galaxy). An isotropic distribution would be horizontal in this plot, and it is clear that the spatial distribution of satellites is significantly anisotropic. Simulated satellites clearly show an "anti-Holmberg" effect, aligning themselves preferentially along the plane perpendicular to the angular momentum axis of the halo.

The effect is significant but relatively weak; satellites along the plane outnumber those closer to the rotation axis by roughly 2:1. The effect depends only very weakly on the luminosity of the primary, as shown in Figure 14, or on the relative brightness of the satellites. We have also checked that the effect is essentially independent of the color of the satellites. Quantitatively, we show this in Table 4, where we report the *average* value of $|cos(\theta)|$ for various combinations of primary/satellite luminosity/color.

A theoretical study of these alignment issues based on an N-body/semi-analytic model similar to but substantially smaller than the Millennium Simulation has recently been carried out by Kang et al. (2007). These authors did not require their primary systems to be isolated, nor did they require a substantial magnitude difference between host galaxy and satellites. As a result it is difficult to compare their results quantitatively with our own. Nevertheless, there are a number of results in common between our two studies. They found that the observed alignments between satellite and central galaxies were best explained by assuming the minor central galaxy to align with the spin of its host subhalo (as assumed here) rather than assuming the major axis of the galaxy to align with that of its subhalo, and they found alignments of similar strength to those we show here. Their model gave dependences of the strength of the alignment signal both on the colour of the host galaxy and on the colour of the satellites. Such trends are weak or absent for the MS samples we study here. This difference is most likely due to the much wider range of systems included in the Kang et al study.

The weak dependence we find of the anisotropy on galaxy properties such as luminosity and color seems at odds with a number of observational studies. Some of them suggest that only satellites of red primaries are anisotropically distributed (Azzaro et al. 2006, Yang et al. 2006, Agustsson & Brainerd 2007), and that the effect is enhanced when considering red companions to red primaries (Yang et al 2006). We note, however, that this result may be affected by the large scatter in the mass-luminosity-color relation discussed in § 3.1. Satellites are typically searched within a fixed radius (of order 500 kpc), a choice that would lead to the inclusion of a larger fraction of interlopers around blue primaries, which
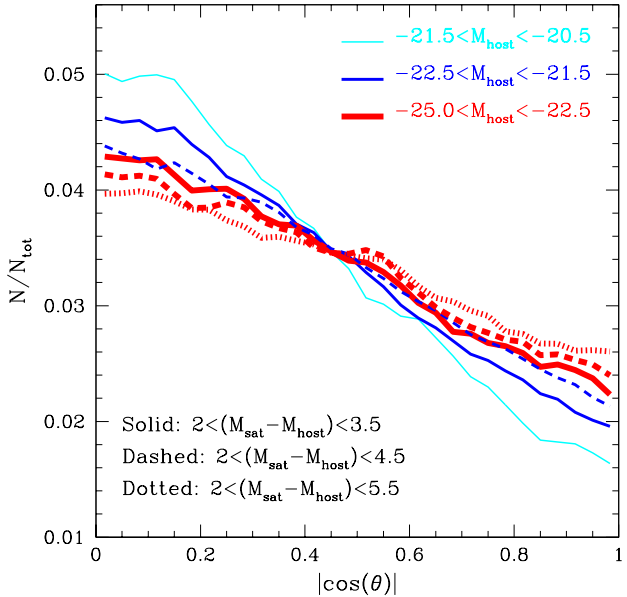

Figure 14. Spatial anisotropy of the satellite spatial distribution, as measured by the distribution of the cosine of the polar angle, $|cos(\theta)|$, measured from the rotation axis of the host halo. Different colors correspond to different primary luminosity, as labelled. Different line types correspond to varying the magnitude range used to select satellites, also as labelled (see also Figure 6). An isotropic distribution would be horizontal in this plot. Satellites show a well-defined "anti-Holmberg" effect; i.e., they tend to populate preferentially the plane *perpendicular* to the angular momentum axis of the host halo.

tend to inhabit halos of lower mass. This may dilute the anisotropy in blue subsamples, explaining the observational results.

A similar comment applies to other potential correlations reported in the literature, such as the trend for spatial anisotropies to decline at large radius (Brainerd 2005; Augustsson & Brainerd 2007) or to increase with halo mass (Yang et al 2006). As this paper was nearing submission, Bailin et al. (2007) argued in a recent preprint that the alignment of satellites may significantly depend on the isolation criteria applied. These authors find that satellites of "truly" isolated SDSS primaries *do* show a polar excess (the original "Holmberg effect"). We have checked for this in our catalogue, but find little dependence of our conclusions on $L_{\text{host}}/L_{\text{sys}}$. A detailed assessment of the correlations claimed by Bailin et al (2007) in light of our results is beyond the scope of this paper, but it is clearly an issue of interest to which we plan to return in future work.

4 SUMMARY AND CONCLUSIONS

We analyse a large sample of isolated galaxies and their satellites selected from the semianalytic galaxy catalogue constructed by Croton et al (2006) from the *Millennium Simulation* (*MS*). The large number of galaxies in the catalogue, together with the large volume surveyed by the *MS*, allow us to characterize in detail the 3D dynamical properties of the satellite population of bright isolated galaxies. Our isolation criterion stipulates that all galaxies within $1\,h^{-1}$ Mpc should be at least 2 mag fainter than the primary.

This criterion typically selects galaxies in sparse environments, but also picks systems of galaxies with peculiar luminosity gaps between the two brightest galaxies, such as "fossil groups".

Our main conclusions may be summarized as follows:

• The relation between the halo mass of isolated galaxies and their luminosity shows very large scatter (halo masses span over a decade in mass at given luminosity), compromising the ability of studies that rely on stacking satellites of galaxies of similar luminosity to probe their dark matter halos. Selecting primaries by color in order to eliminate the reddest and bluest primaries helps to tighten the mass-luminosity relation, but still a number of "underluminous" central galaxies of massive groups remain in the sample. These may, however, be excluded by surveying the environment of the primary and rejecting those in regions of anomalously high richness.

• One corollary of the above conclusion is that the relation between primary luminosity and satellite velocity dispersion is rather sensitive to the primary selection criteria. Stacking all satellites of all primaries leads to an L-σ relation that is poorly approximated by a power law, and much shallower that the $L \propto \sigma^3$ scaling expected for hierarchical models. Only after weeding out massive halos with underluminous central galaxies do we recover the expected $L \propto \sigma^3$ scaling.

• Since our isolation criterion readily selects the central galaxies of "fossil" groups, our analysis may be used to predict the abundance of groups with unusual gaps in the luminosity of the two brightest galaxies. We find that about 8 to 10% of halos exceeding $10^{13}\,M_\odot/h$ would qualify as "fossil" systems, a result that seems consistent with the (so far rather uncertain) observational constraints. We examine recent claims that the luminosity function of "fossil" groups may be difficult to reproduce in the ΛCDM cosmogony but find no obvious discrepancy with observational constraints for the three fossil group luminosity functions in the literature. Further data are needed to settle this issue.

• The density profile of satellites around primaries may be well approximated by an NFW profile that is slightly less concentrated than the average dark matter profile. This conclusion is sensitive to the color of the satellites; red satellites are significantly *more* concentrated than the dark matter; the opposite is true for *blue* satellites. We also find evidence for luminosity segregation in the satellite population; i.e., a weak tendency for satellites near the primary to be brighter than those further away.

• The velocity distribution of satellites is, like the dark matter, dominated by radial motions within the virial radius. The anisotropy is maximal at intermediate radii, becoming gradually more isotropic near the virial radius. This is a result of the radially-increasing contribution of satellites on their first infall onto the primary, a population of objects with rather small dispersion in radial velocity whose contribution raises the importance of tangential motions in the outskirts of the host halo.

• Satellites are distributed anisotropically around primaries, with a well-defined but relatively weak preference for the plane perpendicular to the angular momentum of the halo (an "anti-Holmberg" effect). This is consistent with the latest observational studies, and is a direct result of misalignment between the angular momentum axis and the triaxial structure of dark matter halos.

The characterization of the satellite population of isolated, bright galaxies we present here has several goals: (i) to guide the compilation of primary/satellite systems that minimize the presence of interlopers, (ii) to facilitate the interpretation of observational results, and (iii) to provide predictions that may be used to validate the semianalytic model of galaxy formation applied to the *Millennum Simulation*, as well as, more generally, the hierarchical nature of galaxy assembly. Many of our results are amenable to direct confrontation with observation, and it is to be hoped that such a comparison will provide a number of insights into galaxy formation physics, and perhaps even some challenges to the ΛCDM paradigm.

REFERENCES

Agustsson I., Brainerd T. G., 2007, ArXiv e-prints
Azzaro M., Zentner A. R., Prada F., Klypin A. A., 2006, ApJ, 645, 228
Bailin J., Power C., Norberg P., Zaritsky D., Gibson B. K., 2007, ArXiv e-prints
Bailin J., Steinmetz M., 2005, ApJ, 627, 647
Battaglia G., Helmi A., Morrison H., Harding P., Olszewski E. W., Mateo M., Freeman K. C., Norris J., Shectman S. A., 2005, MNRAS, 364, 433
Belokurov V., Zucker D. B., Evans N. W., Kleyna J. T., Koposov S., Hodgkin S. T., Irwin M. J., and 27 coauthors 2007, ApJ, 654, 897
Belokurov V., Zucker D. B., Evans N. W., Wilkinson M. I., Irwin M. J., Hodgkin S., Bramich D. M., and 26 coauthors 2006, ApJL, 647, L111
Bertschinger E., 1985, ApJS, 58, 39
Bett P., Eke V., Frenk C. S., Jenkins A., Helly J., Navarro J., 2007, MNRAS, 376, 215
Biviano A., Girardi M., 2003, ApJ, 585, 205
Bower R. G., Benson A. J., Malbon R., Helly J. C., Frenk C. S., Baugh C. M., Cole S., Lacey C. G., 2006, MNRAS, 370, 645
Brainerd T. G., 2004a, ArXiv Astrophysics e-prints
Brainerd T. G., 2004b, in Allen R. E., Nanopoulos D. V., Pope C. N., eds, AIP Conf. Proc. 743: The New Cosmology: Conference on Strings and Cosmology Vol. 743 of American Institute of Physics Conference Series, Constraints on Field Galaxy Halos from Weak Lensing and Satellite Dynamics. pp 129–156
Brainerd T. G., 2005, ApJL, 628, L101
Brainerd T. G., Specian M. A., 2003, ApJL, 593, L7

Table 1. Abundance of *primary* galaxies in the *Millennium Simulation* as a function of halo mass. Columns 2 and 3 indicate the median and the rms dispersion of the luminosity that correspond to primaries residing in halos within each mass bin. Columns 4 and 5 show the density ($n_{\rm prim}$) and the fraction ($f_{\rm prim}$) of halos in the Millennium Simulation that host a *primary* galaxy in our catalogue respectively. The last three columns list the contribution to $f_{\rm prim}$ in each mass bin after applying the color cuts shown in Figure 1.

M_{200} [$M_\odot/h$]	$\log(L_r/L_\odot)$ [median]	$\sigma(\log(L_r/L_\odot))$	$n_{\rm prim}$ [$h^3{\rm Mpc}^{-3}$]	$f_{\rm prim}$ %	f_{g-r} (%) < 0.65	f_{g-r} (%) $< 0.95\ \&\ > 0.65$	f_{g-r} (%) > 0.95
$10^{11} - 10^{12}$	10.17	0.15	15.04×10^{-4}	24.7	1.6	21.2	1.9
$10^{12} - 10^{13}$	10.51	0.18	5.50×10^{-4}	72.1	0.6	37.0	34.5
$10^{13} - 10^{14}$	10.85	0.18	8.37×10^{-6}	10.1	0.1	0.3	9.7
$10^{14} - 10^{15}$	11.34	0.16	0.34×10^{-6}	8.3	0.2	0.6	7.5

Table 2. Abundance of *primary* galaxies in the *Millennium Simulation* as a function of r-band luminosity. Columns 2 and 3 indicate the median and the rms dispersion of the halo mass where primaries of a given luminosity reside. Columns 4 and 5 show the density ($n_{\rm prim}$) and the fraction ($f_{\rm prim}$) of galaxies in the Millennium Simulation that are classified as *primaries* in our catalogue respectively. The last three columns list the contribution to each luminosity bin after applying the color cuts shown in Figure 1.

$\log L_r/L_\odot$	$\log(M_{200}/M_\odot)$ [median]	$\sigma(\log(M_{200}/M_\odot))$	$n_{\rm prim}$ [$h^3{\rm Mpc}^{-3}$]	$f_{\rm prim}$ %	f_{g-r} (%) < 0.65	f_{g-r} (%) $< 0.95\ \&\ > 0.65$	f_{g-r} (%) > 0.95
$10.0 - 10.2$	11.75	0.17	9.00×10^{-4}	18.8	1.3	15.03	2.5
$10.2 - 10.4$	11.95	0.20	$6.22 \times 10{-4}$	22.1	0.7	16.5	4.9
$10.4 - 10.6$	12.19	0.23	3.82×10^{-4}	24.8	0.5	16.9	6.1
$10.6 - 10.8$	12.44	0.25	1.39×10^{-4}	18.4	0.9	15.1	7.3
$10.8 - 11.0$	12.64	0.37	2.03×10^{-5}	25.3	5.0	11.7	7.8
> 11	13.34	0.76	3.70×10^{-6}	25.1	15.6	1.92	7.8

Bullock J. S., 2002, in Natarajan P., ed., The shapes of galaxies and their dark halos, Proceedings of the Yale Cosmology Workshop "The Shapes of Galaxies and Their Dark Matter Halos", New Haven, Connecticut, USA, 28-30 May 2001. Edited by Priyamvada Natarajan. Singapore: World Scientific, 2002, ISBN 9810248482, p.109 Shapes of dark matter halos. pp 109–+

Bullock J. S., Dekel A., Kolatt T. S., Kravtsov A. V., Klypin A. A., Porciani C., Primack J. R., 2001, ApJ, 555, 240

Chapman S. C., Penarrubia J., Ibata R., McConnachie A., Martin N., Irwin M., Blain A., Lewis G. F., Letarte B., Lo K., Ludlow A., O'neil K., 2007, ArXiv e-prints

Chen J., Kravtsov A. V., Prada F., Sheldon E. S., Klypin A. A., Blanton M. R., Brinkmann J., Thakar A. R., 2006, ApJ, 647, 86

Colless M., Dalton G., Maddox S., Sutherland W., Norberg P., Cole S., Bland-Hawthorn J., and 22 coauthors 2001, MNRAS, 328, 1039

Croton D. J., Springel V., White S. D. M., De Lucia G., Frenk C. S., Gao L., Jenkins A., Kauffmann G., Navarro J. F., Yoshida N., 2006, MNRAS, 365, 11

Cypriano E. S., Mendes de Oliveira C. L., Sodré L. J., 2006, AJ, 132, 514

De Lucia G., Kauffmann G., White S. D. M., 2004, MNRAS, 349, 1101

De Lucia G., Springel V., White S. D. M., Croton D., Kauffmann G., 2006, MNRAS, 366, 499

Diaferio A., 1999, MNRAS, 309, 610

Diaferio A., Geller M. J., 1997, ApJ, 481, 633

Diaferio A., Geller M. J., Rines K. J., 2005, ApJL, 628, L97

Diemand J., Kuhlen M., Madau P., 2007, ApJ, 657, 262

Diemand J., Moore B., Stadel J., 2004, MNRAS, 352, 535

D'Onghia E., Lake G., 2004, ApJ, 612, 628

D'Onghia E., Maccio' A. V., Lake G., Stadel J., Moore B., 2007, ArXiv e-prints

D'Onghia E., Sommer-Larsen J., Romeo A. D., Burkert A., Ped-ersen K., Portinari L., Rasmussen J., 2005, ApJL, 630, L109

Drinkwater M. J., Gregg M. D., Colless M., 2001, ApJL, 548, L139

Evans N. W., Wilkinson M. I., 2000, MNRAS, 316, 929

Frenk C. S., White S. D. M., Davis M., Efstathiou G., 1988, ApJ, 327, 507

Fukugita M., Shimasaku K., Ichikawa T., 1995, PASP, 107, 945

Gao L., White S. D. M., Jenkins A., Stoehr F., Springel V., 2004, MNRAS, 355, 819

Gavazzi R., Mohayaee R., Fort B., 2006, A&A, 445, 43

Geller M. J., Diaferio A., Kurtz M. J., 1999, ApJL, 517, L23

Holmberg E., 1969, Arkiv for Astronomi, 5, 305

Hopkins P. F., Bahcall N. A., Bode P., 2005, ApJ, 618, 1

Ibata R., Martin N. F., Irwin M., Chapman S., Ferguson A. M. N., Lewis G. F., McConnachie A. W., 2007, ArXiv e-prints

Irwin M. J., Belokurov V., Evans N. W., Ryan-Weber E. V., de Jong J. T. A., Koposov S., Zucker D. B., and 20 coauthors 2007, ApJL, 656, L13

Jing Y. P., Suto Y., 2002, ApJ, 574, 538

Jones L. R., Ponman T. J., Forbes D. A., 2000, MNRAS, 312, 139

Jones L. R., Ponman T. J., Horton A., Babul A., Ebeling H., Burke D. J., 2003, MNRAS, 343, 627

Kang X., van den Bosch F. C., Yang X., Mao S., Mo H. J., Li C., Jing Y. P., 2007, ArXiv Astrophysics e-prints

Kauffmann G., Colberg J. M., Diaferio A., White S. D. M., 1999, MNRAS, 303, 188

Klypin A., Gottlöber S., Kravtsov A. V., Khokhlov A. M., 1999, ApJ, 516, 530

Klypin A., Prada F., 2007, ArXiv e-prints

Koch A., Grebel E. K., 2006, AJ, 131, 1405

Kochanek C. S., 1996, ApJ, 457, 228

Kravtsov A. V., Gnedin O. Y., Klypin A. A., 2004, ApJ, 609, 482

Kroupa P., Theis C., Boily C. M., 2005, A&A, 431, 517

Libeskind N. I., Cole S., Frenk C. S., Okamoto T., Jenkins A.,

Table 3. Moments of the satellite velocity distributions shown in Figures 8 and 9 in several distance bins. The last column show f_{inf}, the fraction of satellites in each radial shell that are in their first approach to the host.

Component	r/r_{200}	mean	sigma (σ)	skewness (ξ)	kurtosis (κ)	f_{inf}
V_r	0.0-0.5	-0.014	0.96	0.025	-0.68	–
	0.5-1.0	-0.072	0.70	-0.002	-0.45	–
	1.0-1.5	-0.133	0.54	0.014	0.23	15%
	1.5-2.0	-0.187	0.51	0.257	2.39	25%
	2.0-2.5	-0.208	0.52	0.687	5.97	36%
	2.5-3.0	-0.179	0.55	0.644	8.22	40%
V_θ	0.0-0.5	0.0	0.45	0.004	0.99	–
	0.5-1.0	0.0	0.39	0.058	1.44	–
	1.0-1.5	0.0	0.49	-0.087	2.30	15%
	1.5-2.0	0.0	0.51	0.143	8.82	25%
	2.0-2.5	0.0	0.55	0.002	16.58	36%
	2.5-3.0	0.0	0.60	0.240	20.35	40%
V_ϕ	0.0-0.5	0.20	0.x55	-0.020	0.48	–
	0.5-1.0	0.25	0.50	-0.240	1.15	–
	1.0-1.5	0.22	0.51	-0.456	2.23	15%
	1.5-2.0	0.15	0.52	-0.387	4.00	25%
	2.0-2.5	0.10	0.57	-0.785	18.23	36%
	2.5-3.0	0.05	0.60	-0.015	15.00	40%

Table 4. Average $|cos(\theta)|$ (where θ is the polar angle measured from the halo angular momentum axis) of all satellites for different bins in host luminosity and color. The last three columns show the values corresponding to three equal-number subsamples: blue satellites ($(g-r)_{\mathrm{sat}} < 0.95$), intermediate color satellites ($0.95 < (g-r)_{\mathrm{sat}} < 1.01$) and red satellites ($(g-r)_{\mathrm{sat}} > 1.01$).

M_{host}	$\langle|cos(\theta)|\rangle$ all	$\langle|cos(\theta)|\rangle$ $(g-r)_{\mathrm{sat}} < 0.95$	$\langle|cos(\theta)|\rangle$ $0.95 < (g-r)_{\mathrm{sat}} < 1.01$	$\langle|cos(\theta)|\rangle$ $(g-r)_{\mathrm{sat}} > 1.01$
$-21.5 < M_{\mathrm{host}} < -20.5$	0.410	0.404	0.408	0.422
$-22.5 < M_{\mathrm{host}} < -21.5$	0.410	0.447	0.441	0.439
$M_{\mathrm{host}} < -22.5$	0.410	0.476	0.463	0.452
$(g-r)_{\mathrm{host}}$				
$(g-r)_{\mathrm{host}} \leqslant 0.65$	0.426	0.437	0.421	0.417
$0.65 < (g-r)_{\mathrm{host}} \leqslant 0.95$	0.428	0.447	0.430	0.436
$(g-r)_{\mathrm{host}} > 0.95$	0.426	0.497	0.458	0.450

2007, MNRAS, 374, 16

Libeskind N. I., Frenk C. S., Cole S., Helly J. C., Jenkins A., Navarro J. F., Power C., 2005, MNRAS, 363, 146

Little B., Tremaine S., 1987, ApJ, 320, 493

Lynden-Bell D., 1982, The Observatory, 102, 202

Macciò A. V., Moore B., Stadel J., Diemand J., 2006, MNRAS, 366, 1529

Mahdavi A., Trentham N., Tully R. B., 2005, AJ, 130, 1502

Majewski S. R., 1994, ApJL, 431, L17

Majewski S. R., Beaton R. L., Patterson R. J., Kalirai J. S., Geha M. C., Muñoz R. R., Seigar M. S., Guhathakurta P., Bullock J., Rich R. M., Gilbert K. M., Reitzel D. B., 2007, ArXiv Astrophysics e-prints

Martin N. F., Ibata R. A., Irwin M. J., Chapman S., Lewis G. F., Ferguson A. M. N., Tanvir N., McConnachie A. W., 2006, MNRAS, 371, 1983

Mateo M. L., 1998, ARA&A, 36, 435

McKay T. A., Sheldon E. S., Johnston D., Grebel E. K., Prada F., Rix H.-W., Bahcall N. A., Brinkmann J., Csabai I., Fukugita M., Lamb D. Q., York D. G., 2002, ApJL, 571, L85

Mendes de Oliveira C. L., Cypriano E. S., Sodré L. J., 2006, AJ,

131, 158

Metz M., Kroupa P., Jerjen H., 2007, MNRAS, 374, 1125

Milosavljević M., Miller C. J., Furlanetto S. R., Cooray A., 2006, ApJL, 637, L9

Mohayaee R., Colombi S., Fort B., Gavazzi R., Shandarin S., Touma J., 2006, in Mamon G. A., Combes F., Deffayet C., Fort B., eds, EAS Publications Series Vol. 20 of EAS Publications Series, Caustics in dark matter haloes. pp 19–24

Moore B., Ghigna S., Governato F., Lake G., Quinn T., Stadel J., Tozzi P., 1999, ApJL, 524, L19

Navarro J. F., Frenk C. S., White S. D. M., 1996, ApJ, 462, 563

Navarro J. F., Frenk C. S., White S. D. M., 1997, ApJ, 490, 493

Navarro J. F., White S. D. M., 1993, MNRAS, 265, 271

Power C., 2006, in Mamon G. A., Combes F., Deffayet C., Fort B., eds, EAS Publications Series Vol. 20 of EAS Publications Series, The Internal Kinematics Of Cold Dark Matter Haloes. pp 29–32

Prada F., Klypin A. A., Simonneau E., Betancort-Rijo J., Patiri S., Gottlöber S., Sanchez-Conde M. A., 2006, ApJ, 645, 1001

Prada F., Vitvitska M., Klypin A., Holtzman J. A., Schlegel D. J., Grebel E. K., Rix H.-W., Brinkmann J., McKay T. A., Csabai I.,

2003, ApJ, 598, 260

Reisenegger A., Quintana H., Carrasco E. R., Maze J., 2000, AJ, 120, 523

Rines K., Geller M. J., Kurtz M. J., Diaferio A., 2003, AJ, 126, 2152

Romer A. K., Nichol R. C., Holden B. P., Ulmer M. P., Pildis R. A., Merrelli A. J., Adami C., Burke D. J., Collins C. A., Metevier A. J., Kron R. G., Commons K., 2000, ApJS, 126, 209

Sales L., Lambas D. G., 2004, MNRAS, 348, 1236

Sales L. V., Navarro J. F., Abadi M. G., Steinmetz M., 2007a, MNRAS, pp 611–+

Sales L. V., Navarro J. F., Abadi M. G., Steinmetz M., 2007b, MNRAS, pp 610–+

Seljak U., Makarov A., McDonald P., Anderson S. F., Bahcall N. A., Brinkmann J., Burles S., and 16 coauthors 2005, PhRvD, 71, 103515

Sommer-Larsen J., 2006, MNRAS, 369, 958

Spergel D. N., Verde L., Peiris H. V., Komatsu E., Nolta M. R., Bennett C. L., Halpern M., 10 coauthors 2003, ApJS, 148, 175

Springel V., White S. D. M., Jenkins A., Frenk C. S., Yoshida N., Gao L., Navarro J., Thacker R., Croton D., Helly J., Peacock J. A., Cole S., Thomas P., Couchman H., Evrard A., Colberg J., Pearce F., 2005, Nature, 435, 629

Springel V., White S. D. M., Tormen G., Kauffmann G., 2001, MNRAS, 328, 726

Strauss M. A., Weinberg D. H., Lupton R. H., Narayanan V. K., Annis J., Bernardi M., Blanton M., and 29 coauthors 2002, AJ, 124, 1810

Trentham N., Hodgkin S., 2002, MNRAS, 333, 423

van den Bosch F. C., Norberg P., Mo H. J., Yang X., 2004, MNRAS, 352, 1302

van den Bosch F. C., Weinmann S. M., Yang X., Mo H. J., Li C., Jing Y. P., 2005, MNRAS, 361, 1203

van den Bosch F. C., Yang X., Mo H. J., Norberg P., 2005, MNRAS, 356, 1233

van den Bosch F. C., Yang X., Mo H. J., Weinmann S. M., Macciò A. V., More S., Cacciato M., Skibba R., Kang X., 2007, MNRAS, 376, 841

Vikhlinin A., McNamara B. R., Hornstrup A., Quintana H., Forman W., Jones C., Way M., 1999, ApJL, 520, L1

White S. D. M., Navarro J. F., Evrard A. E., Frenk C. S., 1993, Nature, 366, 429

Wilkinson M. I., Evans N. W., 1999, MNRAS, 310, 645

Willman B., Dalcanton J. J., Martinez-Delgado D., West A. A., Blanton M. R., Hogg D. W., Barentine J. C., Brewington H. J., Harvanek M., Kleinman S. J., Krzesinski J., Long D., Neilsen Jr. E. H., Nitta A., Snedden S. A., 2005, ApJL, 626, L85

Yang X., van den Bosch F. C., Mo H. J., Mao S., Kang X., Weinmann S. M., Guo Y., Jing Y. P., 2006, MNRAS, 369, 1293

York D. G., Adelman J., Anderson Jr. J. E., Anderson S. F., Annis J., Bahcall N. A., Bakken J. A., Barkhouser R., Bastian S., and 135 coauthors 2000, AJ, 120, 1579

Zaritsky D., Olszewski E. W., Schommer R. A., Peterson R. C., Aaronson M., 1989, ApJ, 345, 759

Zaritsky D., Smith R., Frenk C., White S. D. M., 1993, ApJ, 405, 464

Zaritsky D., Smith R., Frenk C., White S. D. M., 1997a, ApJ, 478, 39

Zaritsky D., Smith R., Frenk C. S., White S. D. M., 1997b, ApJL, 478, L53+

Zentner A. R., Kravtsov A. V., Gnedin O. Y., Klypin A. A., 2005, ApJ, 629, 219

Zucker D. B., Belokurov V., Evans N. W., Wilkinson M. I., Irwin M. J., Sivarani T., Hodgkin S., and 26 coauthors 2006, ApJL, 643, L103

Zucker D. B., Kniazev A. Y., Bell E. F., Martínez-Delgado D., Grebel E. K., Rix H.-W., Rockosi C. M., and 15 coauthors 2004, ApJL, 612, L121